Modulation of downstream prefrontal areas by spatio-temporal optogenetic stimulation of primary somatosensory cortex

Abstract

Perception as well as encoding of sensory stimuli depend on several recurrent networks spanning multiple brain areas. In rats, for example, neurons in prefrontal cortices show reciprocal connections to primary and secondary somatosensory cortex, temporal higher-order sensory areas such as rhinal cortices, as well as to primary and secondary motor cortex. Prefrontal cortex is associated with executive functions and is therefore likely to be important for modulating the information processed in these different loops. In the current study, we are investigating how prefrontal cortex integrates and processes information from primary sensory areas in context of the sensorimotor loop. We have performed a dual approach to our study in which we combined AAV5 directed viral tracing with optogenetic stimulation and high density silicon probe recordings in ketamine anesthetized rats expressing channelrhodopsin-2(ChR2) in primary somatosensory cortex to investigate the S1 efferent projections to high order cortical areas such as M2 and OFC and how prefrontal cortex integrates and processes information from primary sensory areas in context of the sensorimotor loop. We were able to show labeled axons arising from superficial and deep layers of S1 to M2 but not the OFC. LFP recordings were in agreement with the histological analysis and showed evoked responses all across the M2 superficial layers, but no such evoked responses were recorded in OFC. The individual firing pattern of the OFC was not influenced by the optogenetic stimulation, which is in agreement with our previous analysis.

Vlad Constantinescu

Tim Schröder

Sup. Prof. Francesco Battaglia

Introduction

Circuits of Somatosensory Perception

The whisker barrel field (BF) of the rat primary somatosensory (S1) cortex is a commonly used model system for anatomical and physiological investigations of sensory processing and since a lot of experiments describe the neural connections within the barrel cortex, less is known about the input and output projections stemming from the cortical layers of S1 (*Alloway, 2008; Feldmeyer et al., 2013*). The cortical connections of the S1 barrel cortex have been described with the aid of axonal retrograde and anterograde labeling, viral tracing and electrophysiological techniques *(Alloway, 2008; Wiest et al., 2008)* and showed through a considerable number of studies that the S1 barrel cortex projects to the primary motor cortex (M1, *Fabri and Burton, 1991a; Smith and Alloway, 2013)* and primary and secondary somatosensory cortex (*Fabri and Burton, 1991a; Frostig et al., 2008; Sieben et al., 2013*). In addition to the prominent axonal projections from S1 to S2 and M1 on the same hemisphere of the brain, a number of reciprocal projections to other cortical regions have been shown: bilateral projections to perirhinal cortex, projections to ipsilateral orbital cortex and weaker projections to the contralateral somatosensory cortex *(Fabri and Burton, 1991a; Frostig et al., 2008; Sieben et al., 2013 Petreanu et al., 2007) (Fig.1A).* Moreover, the long-range connectivity of the rat S1 extends to higher order cortical areas as well. Anatomical labeling or retrograde and anterograde AAV assisted mapping of projections from the rodent S1 have shown anatomical projections in area 1 of the ipsilateral cingulate cortex but also in the ipsilateral retrosplenial cortex (*Zakiewicz et al., 2014*) and retrosplenial cortex (*Shibata and Naito, 2008).* In addition, other data have shown anatomical evidence in rats suggesting that somatosensory information reaches other cortical areas involved in memory and spatial navigation such as the hippocampus via its projections to the dorsal part of medial prefrontal cortex (mPFC) but also S1 projects to perirhinal cortex which in turn, projects to the entorhinal cortex (*Pereira et al., 2007, M. Diamond et al., 2012*) (*Fig. 1B).*

Interestingly, other experiments have also identified prefrontal high-order cortical areas as targets of long range projections from sensory cortices. Electrical stimulation of somatosensory cortex evoked orthodromic responses in the prefrontal cortex (PFC) lateral area, roughly corresponding to the M2 (secondary motor area), which contained neurons showing responses to electrical stimulation of the S1 cortex *(Golmayo et al., 2003).* Given the fact that the PFC has been strongly associated with executive function, temporal ordering, cognitive processes and autonomic functions *(Kolb, 1984; Neafsey, 1990; Alvarez and Emory, 2006; Schoenbaum and Esber, 2010),* the direct anatomical connections pose subsequent questions about the direct modulatory effect that sensory areas have on the prefrontal cellular ensembles. Furthermore, recent studies using anatomical tracers have indicated evidence for an ordered arrangement of long range projections from PFC to sensory-motor cortex (*Bedwell et al., 2014*), indicating a neurofeedback loop by which the PFC exerts modulatory influence over sensory areas. Therefore, the anatomical distribution of projections between the S1 and the PFC form an ordered pattern of connections through which neurons in motor and prefrontal cortices actively receive input from sensory areas and in turn, send feedback signals back to primary sensory areas (*Mao et al., 2011, Aronoff et al., 2010, Ferezou et al., 2007*). This mechanism of action might be underlying the encoding of sensory information, modulation of sensory stimuli acquisition and subsequently may be involved in active sensory perception. Thus experiments that focus on the functional properties of these neurofeedback loops, which employ a vast array of techniques such as optogenetics and *in vivo* extracellular electrophysiological recordings of neural ensembles, become crucial in our understanding of how these recurrent networks shape and exert modulatory effects on sensory-motor integration.

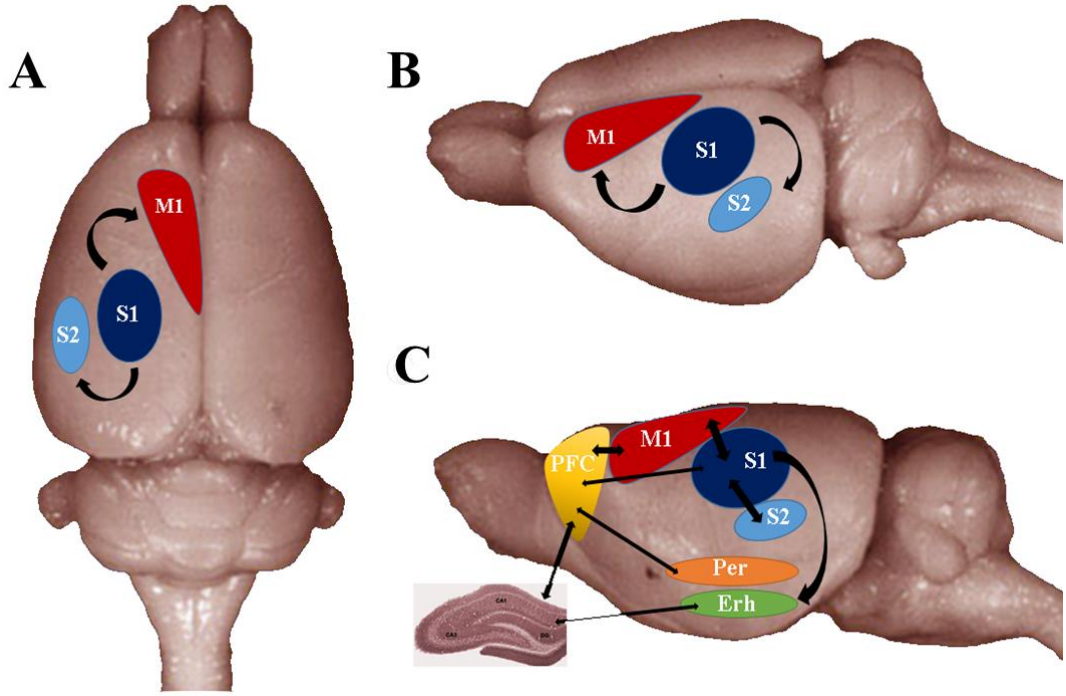

Fig. 1. A (*dorsal view*), B (*lateral view*): *Diagram showing the anatomical and functional connectivity between primary somatosensory cortex (S1, barrel field), secondary somatosensory cortex (S2) and primary motor cortex (M1). The arrows show the flow of information between these cortical areas.* **C:** *Cortical streams from the somatosensory cortex (S1) to a secondary field (SII) with reciprocal connections. Hippocampus (Hipp), PER, perirhinal cortex; ERH, entorhinal cortex; PFC represents the dorsal part of the medial prefrontal cortex.*

S1 connectivity with PFC

Aforementioned data seems to suggest the fact that perception as well as encoding of sensory stimuli depend on several recurrent networks spanning multiple brain areas and that neurons in prefrontal cortices show reciprocal connections to primary and secondary somatosensory cortex as well as to primary and secondary motor cortex. Prominent loops at the level of the cerebral cortex, involving brain regions such as S1, M1 and frontal cortices such as secondary motor area (M2) and orbitofrontal cortex (OFC), which are reciprocally connected, may be involved in the modulation of sensory integration. Furthermore, anatomical tracer studies also revealed that the inputs from OFC and M2 bypass local circuitry and target neurons projecting to brainstem and thalamus. Same studies have also revealed weaker monosynaptic projections from S1 to and from M2 and OFC (*Manita et al., 2015, Bedwell et al., 2014*). Thus, understanding of how much information is conveyed to these downstream areas about the spatial and temporal structure of activity in primary sensory areas becomes crucial in the context of sensorimotor integration. Given the fact that the M2 and OFC are associated with executive functions, are therefore likely to be important for modulating complex behaviours but also modulating the activity of primary sensory areas as well.

S1 connectivity with secondary motor area (M2)

There is a lot of substantial evidence showing that the S1 forms anatomical and functional connections with the M1, by which sensory responsive neurons located in layers II-III and Va of M1 receive somatosensory information directly from sensory-motor projecting neurons found in layers II-III and Va of the somatosensory cortex (*Mao et al., 2011, Aronoff et al., 2010, Ferezou et al., 2007*). The M1 neurons projecting back to the barrel cortex thus exert top-down control over sensory neurons and couple motor and sensory signals, indicating that upper layers in M1 and S1 form a strong feedback loop and participate in forming sensorimotor associations (*Mao et al., 2011*). Despite previous data from anatomical labeling studies which suggest that the same arrangement of connectivity between S1 and M1 is also present between S1 and M2 (*Hoffer et al., 2003; Alloway et al., 2004, 2008; Hoffer et al., 2005; Colechio and Alloway, 2009; Smith and Alloway, 2013*), this feedback loop has received significantly less attention, this due to the fact that it is harder to accurately define the anatomical borders of M2 or because labeling studies reported lesser degree of connectivity between these brain regions when compared to the S1 to M1 sensory-motor loop (*Donoghue and Parham, 1983; Reep et al., 1990; Fabri and Burton, 1991a; Wright et al., 1999; Hoffer et al., 2003; Alloway et al., 2004, 2008; Hoffer et al., 2005; Colechio and Alloway, 2009; Smith and Alloway, 2013*). For example, in rodents, motor cortex is anatomically divided into primary motor cortex (M1) located adjacent to S1, involved in motor control and the more rostral part known as M2 (*Neafsey et al., 1986*), also called medial agranular cortex (AGm), that is linked to higher brain functions including decision making (*Sul et al., 2011*) and self-initiated action (*Murakami et al., 2014*) (*Fig.2*).

Previous studies show indirect evidence that M2 may transmit information to control sensory perception and the subsequent input activity of M2 neuron ensembles to primary sensory areas is hypothesized to modulate perception (*Schneider et al., 2014)*. Moreover, lesions of M2 can produce somato-sensation neglect in rodents (*Vargo et al., 1988*). However, despite anatomical evidence which link S1 and M2, it remained unclear whether M2 input is responsible for sensory stimulus-evoked late activity in S1 and whether these recurrent projections only modulate perception or are critical for active perception as well. To elucidate the anatomical and functional properties of this cortico-cortical neurofeedback loop, in 2015 Manita et al. identified a functional projection between M2 and S1 which underlies a top-down control circuit in the mouse somatosensory system. The authors induced evoked early neural activity in S1 by hind-paw electrical stimulation and were able, using wide-field cortical voltage-sensitive dye imaging (*Ferezou et al., 2007*), to observe a subsequent response in an anterior medial area known in mice as the secondary motor area (M2) (*Paxinos and Watson, 1998*). Furthermore, the location of the sensory responsive area could be clearly distinguished from forepaw M2 and vibrissal M2 cortices, indicating somatotopic map within M2, analogous to S1 and M1.

Further viral tracing experiments revealed direct anatomical projections to both the upper and lower layers of S1 and subsequent electrophysiological recordings showed a correlation between top-down signals and sustained dendritic activity in S1 layer V (LV) pyramidal neurons. Finally, optogenetic inactivation of the top-down projection from M2 to S1 demonstrated that top-down input does not merely modulate perception but can have a direct role in the formation of accurate somatosensory perception (*Manita et al., 2015*). Manita et al. were able to show, using a vast array of techniques, a cortico-cortical neurofeedback loop for top-down control in mouse somatosensory cortex, including its physiological mechanism and role in sensory perception. Their model suggests that sensory information travels to S1 from thalamus, which then relays the early phase of output to other brain areas, including M2. Although a direct implication of this circuit in conscious perception cannot, for the time being, be described, *Manita et al., 2016* showed not only that the M2 to S1 top-down connection drives layer 5 (L V) dendritic spiking during the late component, and that this is required for accurate tactile sensory perception but also how this methodology

can be used to characterize the anatomical and functional properties of cortico-cortical recurrent networks that span throughout the brain. Since sensory cortices show connections to high order cortical areas such as M2 and the OFC, which has been implicated in executive functions, it becomes important to investigate the role that these connections have in modulating the activity of high order cortical areas.

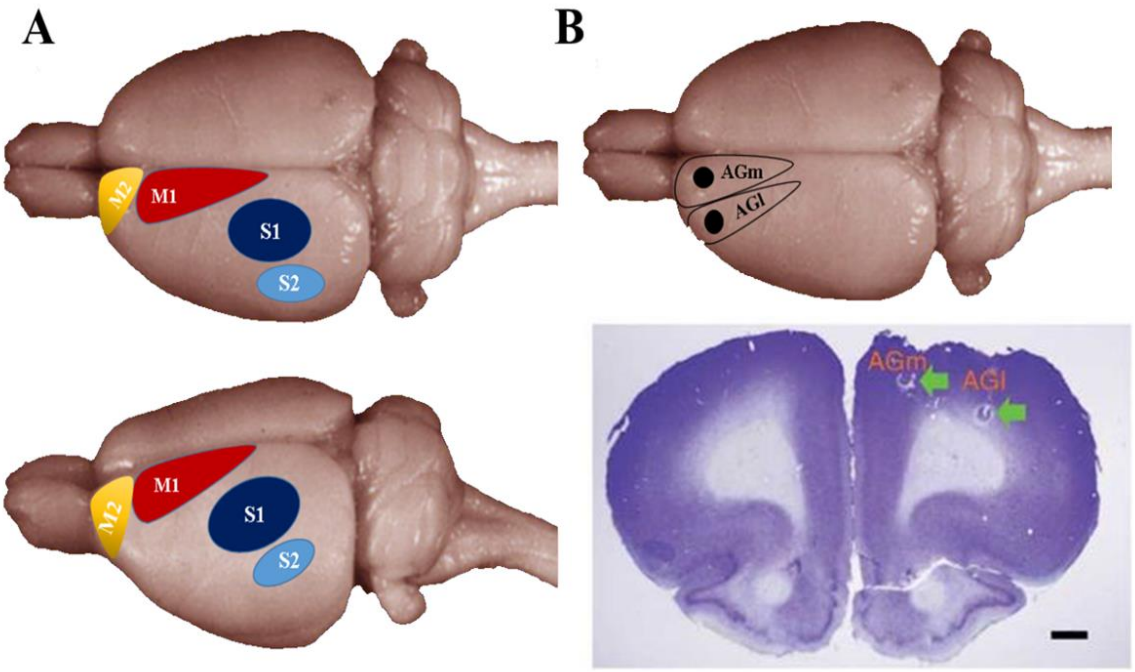

Fig. 2. *Schematic representations showing anatomical overlap between areas described as* **A:** *secondary motor area cortex (M2) and* **B:** *medial agranular cortex (AGm). AGl: lateral agranular cortex;*

S1 connectivity with the orbitofrontal cortex (OFC)

Anatomy of rodent OFC

As it is the case with M2, defining the anatomical borders of the OFC has received quite a lot of attention from the scientific community. The major difficulty in accurately describe this region stems from the fact that, when compared to humans and primates, the rat prefrontal cortex is composed exclusively of agranular cortical areas. Usually, the OFC has been defined topographically as the cortex on the ventral surface of the frontal lobe. However, the definition does not take into account obscure distinct connectional and functional systems within the orbital cortex, thus interpretations of data on the orbital cortex that do not take these different systems into account can become misleading (*Price et al., 2007*). Previous studies have tried to tackle this issue by proposing that equivalent areas could be recognized in different species on the basis of similar connections. In one study (*Rose and Woolsey, 1948a*), the authors hypothesized that the OFC of rabbits and cats was similar to the primate prefrontal cortex due to its connections with the mediodorsal thalamic nucleus and based on this criteria the prefrontal cortex in rats should comprise the following structures: the medial frontal cortex (around and rostral to the genu of the corpus callosum), the cortex at the dorsomedial corner of the hemisphere, and the "orbital" cortex in the dorsal bank of the rhinal sulcus. Unfortunately, this study did not provide a clear answer on the question of which areas in the rat are

homologous to the rostral or dorsolateral granular prefrontal cortex in primates. Also it did not take into consideration that the cortical region which is described as prefrontal cortex may include cortical areas in primates (the rostral and dorsolateral granular areas) that are not present in rodents. Subsequent studies (*Krettek and Price, 1977*) using cytoarchitectonic and connectivity methodologies were able to divide and describe the caudal and ventromedial areas of the prefrontal cortex (all but the rostral parts of the OFC) and subdivided this region into lateral orbital, ventrolateral and medial orbital areas (LO, VLO, MO) (*Fig.3*).

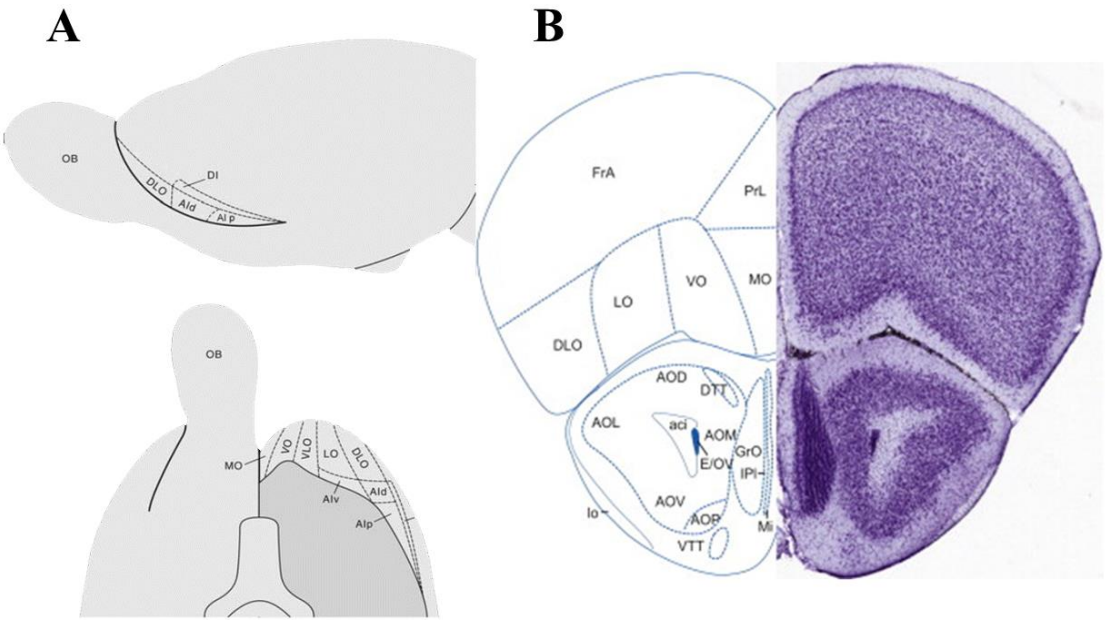

Fig. 3. *Anatomical profile of the orbitofrontalcortex (OFC) based on cytoarchitectonic and connectivity data.* **A:** *upper side medial view, lower side ventral view;* **B:** *Coronal section showing the cytoarchitectonic and anatomical distribution of the OFC subdivisions; OB – olfactory bulb; VO - ventral orbital cortex; DLO – dorso-lateral orbital cortex; AIv, Aid, Aip – ventral, dorsal and parietal agranular insular areas as described by* ***Price et al., 2007.***

Moreover, in other studies (*Price, 2007*) based on analysis of cortico-cortical connections between areas in the orbital and medial prefrontal cortex, the author describes the existence of two distinct networks in this region: one system, which has been named the medial prefrontal network although it includes areas on the medial wall, in the medial orbital cortex, and in the posterolateral orbital cortex and the second system called the orbital network which spans throughout the central orbital cortex. The distinction between these two adjacent brain areas was based on the pattern of connectivity these regions have with other brain structures. The medial network connects to a cortical circuit that includes the rostral part of the superior temporal gyrus and dorsal bank of the superior temporal sulcus, the cingulate and retrosplenial cortex, the entorhinal and posterior parahippocampal cortex, and the dorsomedial prefrontal cortex. The orbital network receives several sensory inputs, from olfactory cortex, taste cortex, somatic sensory association cortex, and visual association cortex, and is connected with multisensory areas in the ventrolateral prefrontal cortex and perirhinal cortex. Also there is evidence that suports the fact that some of these areas are involved in both networks. Although these studies provide a solid anatomical blueprint of the rodent PFC and subdivisions (OFC, mPFC) based on connectivity patterns and cellular laminar distribution, they fail to deliver a comprehensive detailed map of the ordered physiological organization of PFC regions. In a recent study, *Kondo and Witter, 2014*, described a topographic organization of the projection from

orbitofrontal cortex to the parahippocampal region in rats. The authors demonstrated an ordered arrangement of output connections from PFC sub-regions MO, VO, LO to areas of perirhinal, postrhinal and entorhinal cortex but this ordered arrangement was reported only for the output projection.

OFC connectivity with sensory and motor cortices

Despite numerous advances in our interpretation of PFC function in the rat, the functional connectivity patterns of the PFC cannot be fully understood due, in part, to the fact that the precise neuronal circuitry of PFC regions remains largely unknown. So, in order to probe the functional connectivity of the PFC and it's subdivisions it is necessary to first gain a more detailed picture of the underlying anatomical organization. In 2014, *Bedwell et al.* performed an anatomical study using retrograde and anterograde neuronal tracers which were injected into the PFC sub-regions prelimbic (PL), VO, VLO and DLO. The authors were able to observe in their results the patterns of labeling throughout the brain using light and fluorescence microscopy. Injections of retrograde neuronal tracers in these areas produced labeled cells seen in M2, M1, S1, cingulate cortex (Cg1), piriform cortex (Pir), perirhinal cortex (PRh), ectorhinal cortex (Ect), lateral entorhinal cortex (LEnt), secondary auditory cortex (AuV) and primary auditory cortex (Au1). Anterograde neural tracer injections in the PFC subdivisions showed labeled cells in M2, S1, S2, Cg1, PRh, Ect, Lent and agranular insular cortex (AID). Also, an ordered spatial arrangement was seen when labelled cells produced by an injection of retrograde tracer into DLO appear in layer VI, whereas those produced by an injection of tracer into VLO appear in layer V in the same region. Cells labelled following an injection of tracer into VO appear across layers II to VI (*fig. 4*).

As it was the case with the *Kondo and Witter, 2014* study, the authors here also identify a topographic organization of the input and output projections from the PFC. Based on a previous model of hierarchical organization within the cortex, which puts the PFC at the top of the processing hierarchy (*Fuster, 2001; Botvinick, 2008*), the reciprocal connections seen here between the PFC and M2 and M1 are consistent with what would be expected: the connections travel from S1 to S2 and other association areas such as Prh cortex to PFC while return connections would travel to M2 followed by M1. However, the direct connection from S1, a primary cortical region, to high order sub-divisions of PFC, was unexpected, leading the authors to hypothesize the existence of an atypical circuit within the sensory-motor cortices and the PFC. The most notably feature of this circuit pattern is that specific layers of M1 and S1 (layers V and VI) differentially project to prefrontal targets VO and VLO. This arrangement of projections from sensory and motor areas could be of significance to PFC function because both of these regions (M1 and S1) contain somatotopic maps, and thus the transfer of information would be facilitated if the PFC maintains the same ordered arrangement of connections with the sensory and motor cortices. This type of cortical arrangement was also observed during electrical stimulation experiments (*L. Golmayo et al., 2003*). Here, the authors show that electrical stimulation of layer V of either S1 or the visual cortex evoked neural responses in two distinct regions of the PFC. A lateral area, roughly corresponding to the M2, contained neurons showing responses to electrical stimulation of the somatosensory cortex and a medial area, located in the rostral part of the cingulate cortex (Cg1), that responded to electrical stimulation of the visual cortex. However, here the authors described different convergence points for this two pathways. While stimulation of the S1 span throughout the posterior-anterior axis of M2, only visual stimuli from the V1 in rats reached the orbitofrontal cortex. These functional observations add to the already growing body of anatomical evidence which highlight that a level of hierarchy within the PFC connectivity must be maintained for accurate sensory perception.

Contrary to these findings, also in *2014, Zakiewicz et al,* performed a detailed analysis of the efferent projections of the rat barrel cortex in which, after anterograde tracers were injected in whisker S1 or forelimb cortex, the authors describe anatomical differences between S1 whisker and forelimb related

projections. Even though most of the efferent projections matched previous experiments, the study failed to show a direct connection in both cases (whisker/fore-paw) between the sensory areas and the OFC. This difference can be attributed to the fact that the *Zakiewicz et al* study S1 injections targeted the L IV barrel corresponding to the C2 cortical representation directly in the BF and the previous mentioned data shows a reciprocity between S1 and OFC in L V and VI but also layers II-III, bypassing the barrel circuitry. This difference also poses a very interesting hypothesis, in which the amount of information that is relayed from S1 to the PFC covers distinct and different projection patterns.

Nevertheless, the anatomical and functional connections highlighted by these studies indicate a broad reciprocal organization between sensory-motor cortices (S1, M1 and M2) and the PFC. Even though these findings only add another level of complexity to this area by highlighting the connections of orbital cortex to motor cortex and the newly described, indirect input of somatosensory cortex to motor cortex (via the orbital PFC), understanding how much information is conveyed to these downstream areas about the spatial and temporal structure of activity in primary sensory areas becomes crucial in the context of sensorimotor integration. Given the fact that the M2 and OFC are associated with executive functions, are therefore likely to be important for modulating complex behaviors but also modulating the activity of primary sensory areas as well.

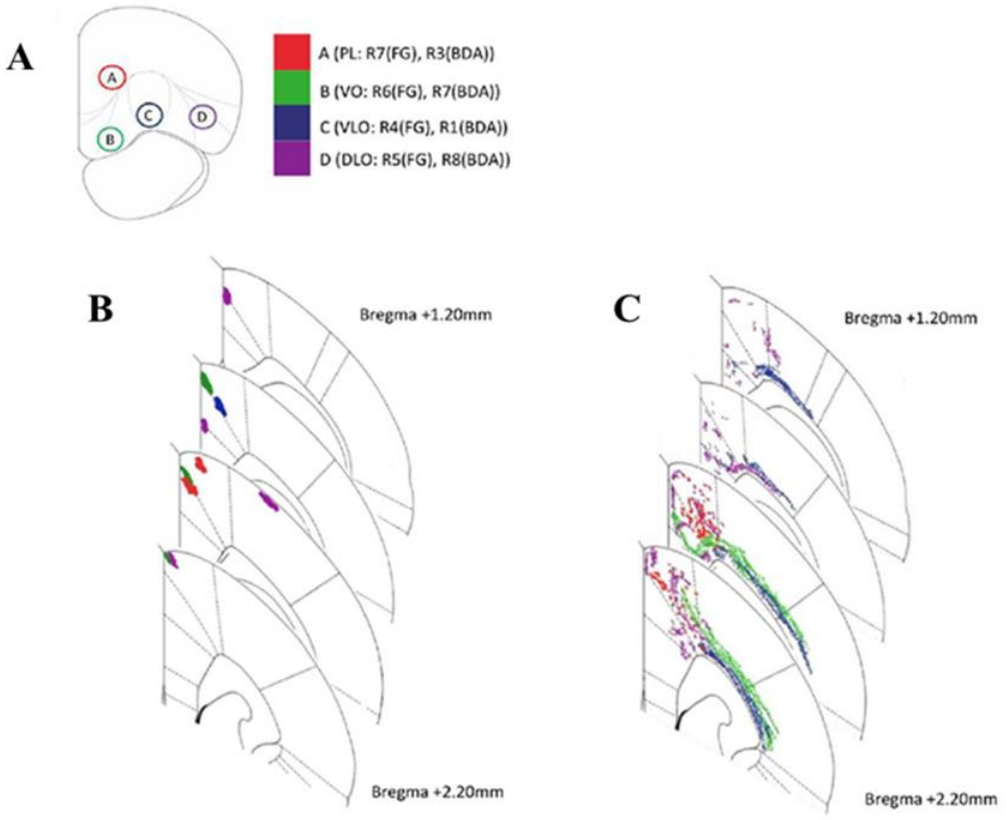

Fig. 4. *Coronal sections depict the injection site and projecting sites*. **A:** *The positions of four injection sites within PFC; PL (injection A), VO (injection B), VLO (injection C) and DLO (injection);* **B:** *Anterograde labeling of axon terminals (PFC output connections) following injections into four PFC sites;* **C:** *Retrograde labeling (PFC input connections) following injections into three PFC sites as described by Bedwell et al, 2014.*

Optogenetics and electrophysiological approaches

As highlighted by the study mentioned before, the advances in the development of anatomical and viral neural tracers allow us to investigate the pattern of connectivity between brain areas in high resolution, having more access to the underpinnings of cortico-cortical circuits. The results presented in this experiment (*Bedwell et al., 2014*) elegantly show the intricate pattern of connectivity the PFC has with the sensory-motor and premotor areas. Moreover, the authors were able to describe direct projections from primary sensory areas to the rat PFC subdivisions (also described in mouse models, *Aronoff et al, 2010, Mao et al., 2011*) which added another layer to the complexity of cortico-cortical loops. However, describing the functional properties of such cortical loops becomes impossible with only anatomical data. To accurately describe the underlying mechanism by which each brain region exerts modulatory effects on other areas in the context of the sensorimotor loop, a different methodological approach must be used. Distinct anatomical areas that span across the cortex have different stimulatory and inhibitory effects on downstream targets, thus targeting specific brain regions during functional connectivity experiments is a must. There are several techniques employed for isolation and subsequent excitation or inhibition of specific cellular subsets such as chemogenetics and optogenetics. The latter has received more attention from the scientific community in the last decade. Optogenetics is a branch of biotechnology that combines genetic engineering, optics, and light-sensitive molecules to achieve precise control of cell activity. In this method, illumination of natural or synthetic photoreceptor proteins changes their conformation, leading to activation or inhibition of the host cell. The hallmark of optogenetics therefore is introduction of fast light-activated channels, pumps, and enzymes that allow temporally precise manipulation of electrical and biochemical events while maintaining cell-type resolution through the use of specific targeting mechanisms. Among the microbial opsins which can be used to investigate the function of neural systems are the channelrhodopsins (ChR2, ChR1, VChR1) (*Nagel et al., 2002, 2003; Kato et al., 2012; Deisseroth 2006*) to excite neurons and anion-conducting channelrhodopsins for light-induced inhibition.

Light-driven ion pumps are also used to inhibit neuronal activity, halorhodopsin (NpHR), enhanced halorhodopsins (eNpHR2.0 and eNpHR3.0) (*Deisseroth et al., 2009*) (*fig. 5*). Optogenetics also includes the development of genetic targeting strategies such as cell-specific promoters or other customized conditionally-active viruses, to deliver the light-sensitive probes to specific populations of neurons in the brain of living animals (worms, fruit flies, mice, rats, and monkeys). Another aspect to be taken into consideration when performing such experiments is the capacity to record simultaneously the activity of different subsets of neurons in real time. To capture the fast events that take place at a synapse level, electrophysiological measurements are employed. Electrophysiology is the study of the electrical properties of biological cells and tissues and it includes measurements of the electrical activity of neurons, and, in particular, action potential activity. This technique comes in a variety of forms and protocols ranging from intracellular recordings measuring voltage and/or current across the membrane of a cell (voltage/current clamp) to extracellular recordings *in vivo* of single and multi-units as well as local field potentials. Extracellular recordings are used to monitor neuronal activity from outside the cell and it provides a means to measure patterns of action potentials within many areas of the peripheral and central nervous systems. In addition, massed activity can also be recorded in the form of local field potentials which are local current sinks or sources that are generated by the collective activity of many cells. With the development of high density silicon probes that incorporate up to hundreds of channels, we can now use these tools to record spatio-temporal characteristics of the electrical signal ranging from single extracellular units, or spike activity, to multi-unit activity to neuronal activity that gives rise to transmembrane current and the summation of these currents referred to as local field potential (LFP), with unprecedented resolution.

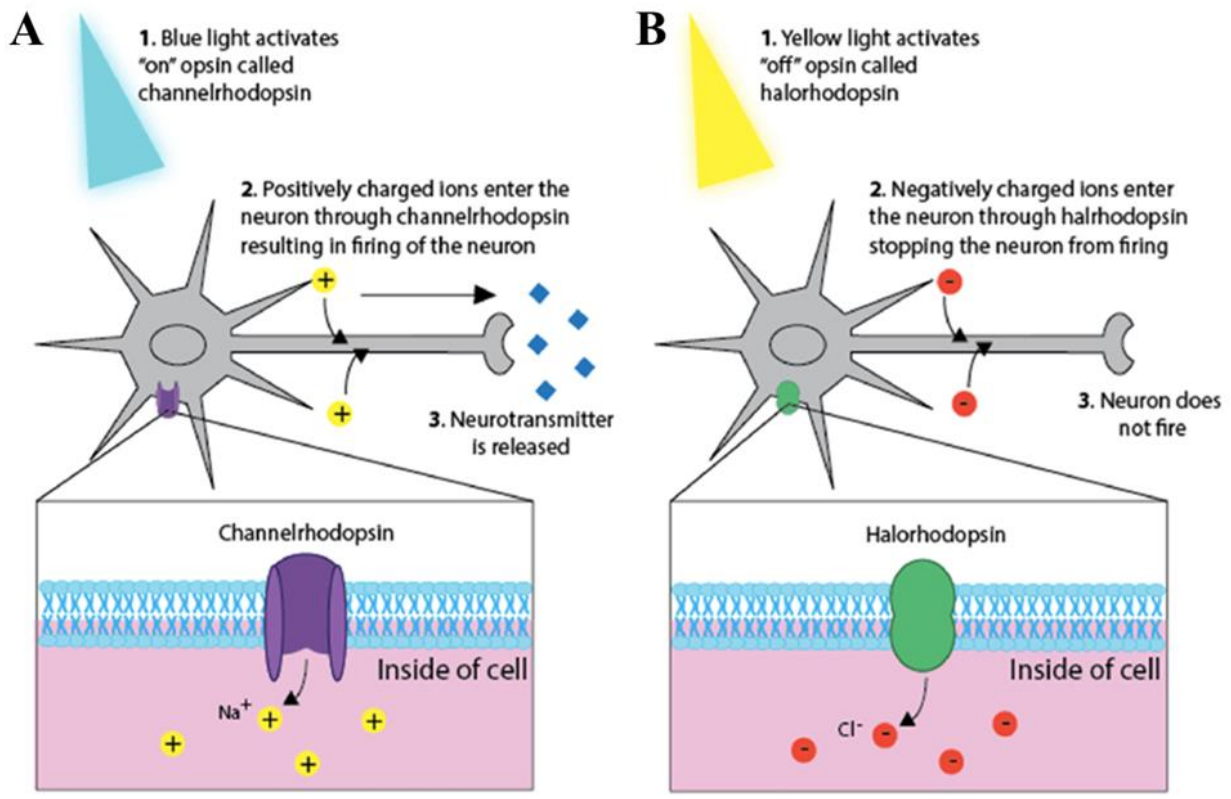

Fig. 5. S*chematic representation of the the mechanism of optogenetic stimulation/inhibition*. **A:** *Neural excitation provided by the stimulation of channelrhodopsin 2 by a flash of blue light results in firing of the neuron and subsequent neurotransmitter release;* **B:** *Neural inhibition provided by the stimulation of halorhodopsin ba a flash of yellow light stops the neuron from firing action potential and subsequent neurotransmitter release.*

Project Aim

Based on the amount of data presented before, it becomes clear that the ordered pattern of connectivity within the PFC and in the sensory-motor cortex (S1, M1 and M2) is involved in the accurate integration of sensory-motor stimuli within the cortex. As seen before, the reciprocal connections the S1 shares with the M1 and M2 form a neurofeedback loop by which both M1 and M2 exert a top-down modulatory effect on S1. Interestingly, this top-down effect was proven to have a very important role in accurate sensory perception (*Mao et al., 2011; Manita et al., 2016*). Moreover, the same ordered arrangement was also described for the medial and orbital sub-regions of the PFC. The orbital network receives input from M1 and M2 via direct topographically distinct projections and sends back projections to these regions thus completing the neurofeedback loop (*Bedwell et al., 2014*). However, this reciprocity was not seen in the newly described direct projections from S1 to sub-divisions of the PFC. Here, labeling from retrograde injections made into OFC was considerably more widespread than that from anterograde injections, therefore the connections are not reciprocal. The deep layers of S1 send direct information to regions of the OFC, bypassing the immediate connections S1 shares with M1 and M2, but the direct reciprocal connection from OFC to S1 is considerable lower. This may indicate that the amount of information exchange between these areas differs from the one that takes place between sensory-motor cortex and the PFC. Thus, in this context, it becomes highly important to describe the modulatory effects of sensory stimuli that directly have an influence on the OFC activity.

In the current study, we aimed at investigating firstly how the pattern of connections from the supra- and infragranular layers of the S1 cortex project to downstream cortical areas using an adeno-associated (AAV5) viral tracing but more important how prefrontal cortex integrates and processes information from primary sensory areas in context of the sensorimotor loop. In ketamine anesthetized rats expressing channelrhodopsin-2(ChR2) in primary somatosensory cortex, we used an array of epidural micro-LEDs to excite principal neurons in S1 in distinct spatio-temporal patterns. Simultaneously, we recorded local field potentials, single and multi-unit responses in primary motor cortex, secondary motor cortex, orbitofrontal, or prelimbic cortices using high density silicon probes with up to 128 channels.

Materials and methods

Animals

Data was collected from 2 (+2 control animals) male Long Evans rats (400-450g, Charles River, United Kingdom) for the electrophysiological recordings and 3 animals for viral tracing study (350g, Charles River, United Kingdom). The animals were housed under controlled environmental conditions. The temperature was 20±2º C and the humidity was 50±10 %. The animals had ad libitum access to standard laboratory chow and autoclaved water. Environmental enrichment was provided in the form of wooden chew blocks. Animals were housed two rats/cage before and after surgery. The animals were housed with a 12:12 light: dark cycle with lights off at 10:00 am following an acclimation period of one week due to transport stress and habituation to the dark/light cycle. Before surgery animals were handled and weighed twice a week at the end of the light phase to assess general health. After surgery animals were weighed and handled every day. The animals were examined for clear signs of ill-health (infections, signs of pain) or behavioral change immediately prior to surgery and after the surgery. There were no observed clinical symptoms of toxicity or infection. There was no significant effect on body weight development detected. All experiments were approved by the local animal experiment and welfare committee (Dier Experimenten Commissie, Centrale Commissie Dierproeven-CCD) of The Netherlands.

Surgical procedures

- **Viral vector injection**

An adeno-associated virus (AAV5-CamKII-ChR2-EYFP) was selected in order to limit the viral expression to excitatory neurons due to its CamKII promoter. The animals were administered a pre-surgery saline injection (3ml) subcutaneously to prevent dehydration during the surgery and anesthetized using a mixture of ketamine, saline, and atropine (ratio 11:2.5:1.5, dose 1ml per kg body weight) and restrained in a stereotactic apparatus (Robot Stereotaxic, Neurostar, Tübingen, Germany) equipped with an automated drill which was fitted with a 35 gauge Hamilton 1 ml syringe for automatic injection. Before the scalp incision, animals were injected with lydocaine, a local anesthetic. The scalp was disinfected using Povidone Iodine. An incision was made above the skull. After removing the periosteum to allow for accurate identification of Bregma coordinates, two injection holes were prepared on the skull unilaterally above the left primary somatosensory cortex (S1, coordinates: posterior, -2.04 and -1.04 mm and lateral, 4.3 mm, Paxinos&Watson 6th edition) using the automatic drill with a drill bit diameter of 0.8 mm. The Hamilton syringe was lowered into the brain tissue to the deep layer of the S1 cortex and a 20 min time was allowed to prevent anatomical distortion of brain areas. Subsequently, the viral construct was injected unilaterally into the left hemisphere with the aid of an electronic injectomat. Each 500 µl injection (100-150 µl per min) was into deep layers of S1. Following the viral construct delivery to the brain tissue, a post injection period of 10 min was allowed to make sure the viral construct diffuses and reaches the area sufficiently. After the

needle was removed, the skin was sutured. Following surgery, the animals were administered a second injection of saline (3ml) weighed daily and checked for signs of ill-health (infections, signs of pain) or behavioral change until recovery. Throughout the procedure, body temperature was maintained and heart rate was monitored.

- **Silicon probe recordings**

Surgery

After allowing a 3-4 weeks recovery period after the viral injection and subsequent viral expression of the opsin, the AAV-injected Long Evans rats underwent silicon probe recordings. The animals were anesthetized at the beginning of the surgery using a combination between a mixture of ketamine (1,1ml), saline (0.25 ml) and atropine (0.15 ml) and Dexmedetomine (Dexdomitor) was administered in a concentration of 1 ml/kg of body weight and restrained in a stereotactic apparatus for the duration of the recording procedures. Throughout the surgical procedure anesthesia was maintained throughout the experiment by additional doses of ketamine (1,1ml), saline (0.25 ml) and atropine (0.15 ml) at one hour intervals at a volume of 0,5ml/kg. An incision was made above the skull. After removing the periosteum to allow for accurate identification of Bregma coordinates, craniotomies were prepared on the skull unilaterally above the desired locations using a hand-held drill with a drill bit diameter of 0.8 mm. To allow space for the LED optogenetics stimulation grid (*see Optogenetic stimulation*) to fit over the S1 stimulation area containing the barrel field, the craniotomy over the S1 was substantially larger in size compared to our prefrontal recording sites (craniotomy over S1: from -4,5 to -1.05 mm posterior and -2 to -5,5 mm medial to Bregma). Given the anatomical distribution of our desired recording sites, only one prefrontal craniotomy was performed. The craniotomy above the recording sites, the primary motor cortex (M1), premotor cortex (M2), prelimbic area (PL) and orbitofrontal cortex (OFC), spanned from 2 to 5 mm anterior and -1 to -4 medial from Bregma . The array of µLEDs was placed above the S1 cortex between above the dura mater (*fig. 6A*), at 1mm anterior to the previous viral injection site. The array was anchored after placement, using dental cement, on the rat's skull (*fig. 6B*). Before the silicon probe was implanted, to allow for accurate histological localization, we applied a fluorescent lipophilic dye (DiL) over the silicon probe. A single metal screw was attached to the skull above the cerebellum (3mm posterior to Lambda coordinates) to ensure a reference reading for the signal but also to minimize the electrical noise. A single shank silicon probe (*NeuroSeeker, IMEC, Belgium*) *(fig. 7)* containing 128 recording sites was lowered in the left hemisphere at different locations in the prefrontal cortex: coordinates relative to Bregma: Motor cortex (M1) (anterior 3.2 mm, lateral 3.4 mm and ventral 2.6 mm), premotor area (M2) (anterior 3.7 mm, lateral 1.8mm and ventral 2.4 mm), prelimbic (PL) (anterior 3.2 mm, lateral 0.6 mm and ventral 3.4 mm) and orbitofrontal cortex (OFC) (anterior 4.2 mm, lateral 1.8 mm and ventral 4.5mm) (*fig. 10*). Following the probe implant, a 20 min time was allowed to prevent anatomical distortion of brain areas. After the recordings were finished, the probe was removed in 50 µm steps to limit tissue damage. Throughout the procedure, body temperature was maintained and heart rate was monitored.

Recording

All data was acquired using a multi-channel digital acquisition system (*Open Ephys acquisition board*). The acquisition board works automatically with the Open Ephys GUI integrated and open source software, which allows for visualization and analysis of data in real time. We recorded the broadband signal (1-7500 Hz, filtered on the two RHD2164 64-Channel Amplifier Boards) and separated the signal in single/multi-unit activity and LFP during subsequent analysis (*see Signal Analysis)*. The silicon probe was used to record simultaneously local field potential (LFP), multi-unit activity (MUA) and single unit activity.

The data was acquired during a 20-min baseline recording session without stimulation, 60-min recording period with stimulation, and 20-min post-stimulation period.

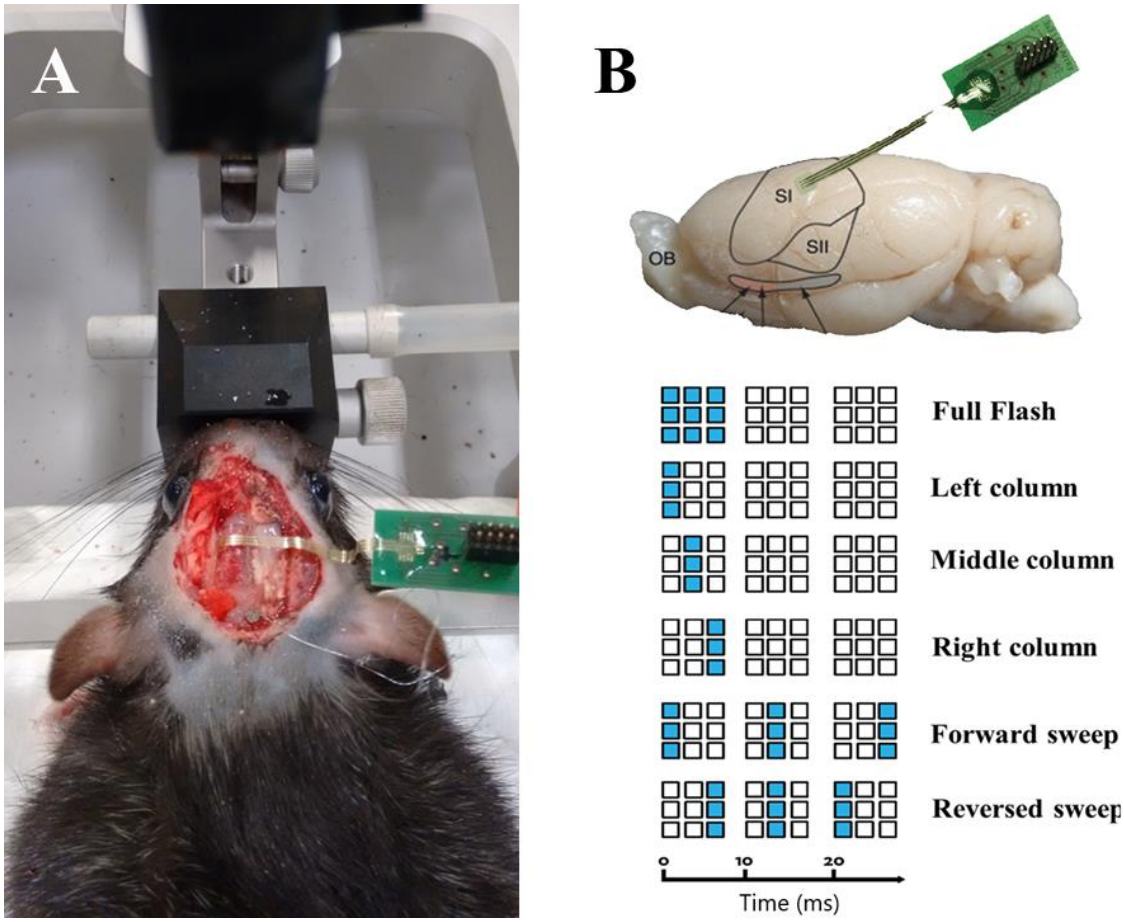

Fig. 6. A: *Optogenetic stimulation setup and anchoring of the LEDs array to the skull*. **B upper panel:** *Localization of the LED array over the cortex;* **lower panel:** *Pattern of light stimulation;*

Histological analysis

After the recording experiments were finished, animals were deeply anesthetized with sodium-pentobarbital (50 mg/kg) and then perfused transcardially with saline followed by paraformaldehyde (PFA) (4% in saline). The brain was removed, washed repeatedly for three days with 0.01M Phosphate buffer (PB) and stored in 30% sucrose phosphate buffered saline solution for 24 to 36 h until the brain dropped to the bottom of the cup. After freezing with dry ice, the brains were cut on a Leika freezing cryostat. Coronal sections 50 µm thick were stained with an Anti-GFP antibody (Abcam lab.), or the Nissl method to locate the recording sites. To visualize the slices, we used a Leika Spx8 confocal microscope, and pictures were taken and stitched together using the in-built microscope software. The aim of the histological analysis was to accurately identify the sites of viral opsin expression in the neural tissue. Following the first viral injections, the histological analysis revealed areas of overexpression in the brain tissue but also opsin expression was seen in layer IV of the S1 (*fig. 8 A*), which covered the BF of the rat S1, most likely due to the amount of viral construct we injected (1 injection with 1000 µl). Given the fact that the majority of projections between the S1 and M1, M2 and PFC arise from superficial and deep layers of S1 (L II-III and V), in this study we aimed at opsin expression to these cortical layers only. This was achieved by two injections in the deep layer of S1 separated by 1mm distance (*fig. 8 B and C*).

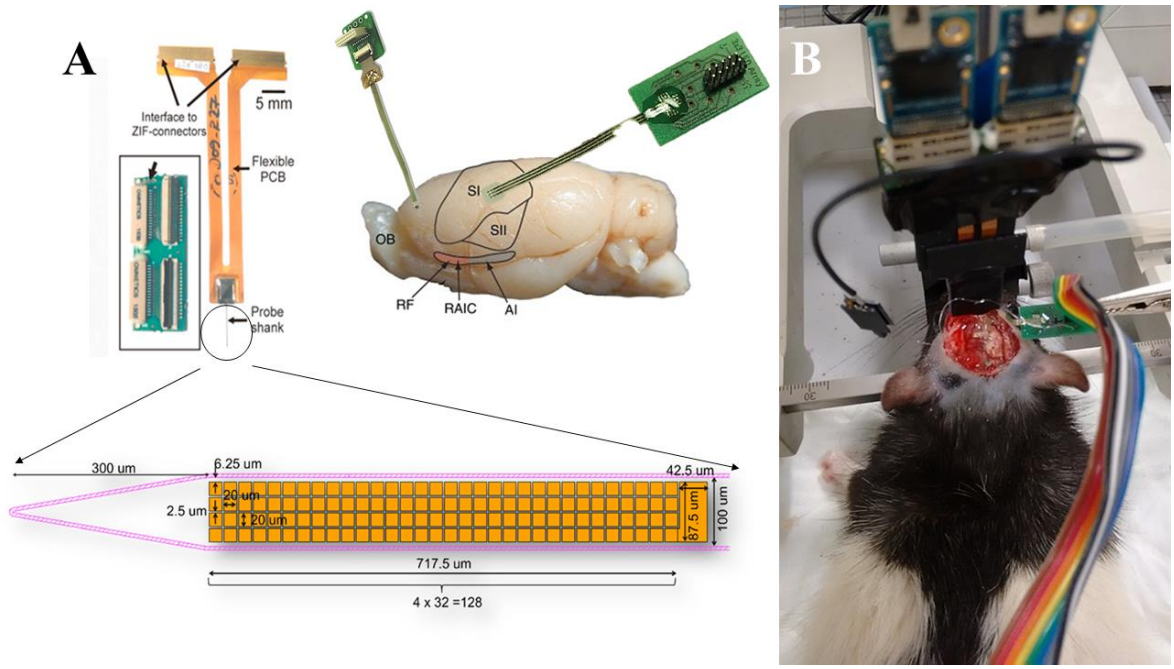

Fig. 7. A: *NeuroSeeker silicon probe. Microelectrode arrays based on complementary metal-oxide semiconductor. NeuroSeeker probes provide 128 recording sites on an extremely narrow shank, with on-board amplification, digitization, and multiplexing;* **B:** *Schematic representing the localization over the cortex and electrophysiological recording setup of the Neuroseeker silicon probe shank;*

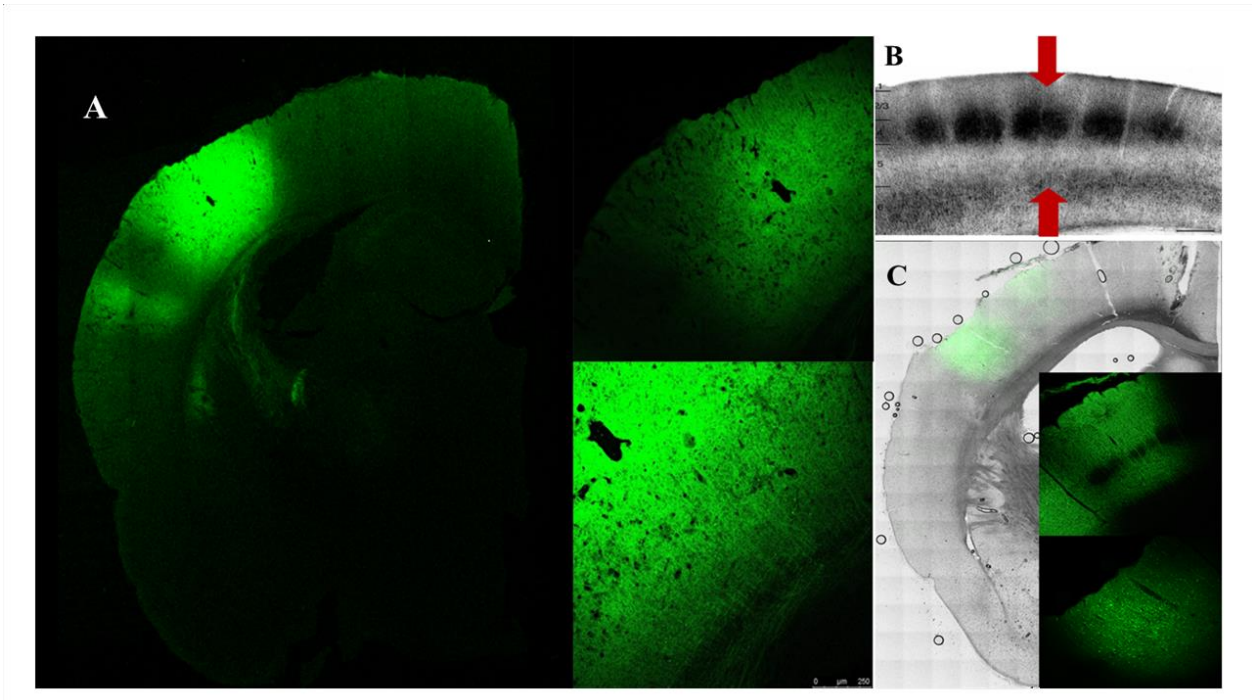

Fig. 8. A: *Picture is showing the areas of overexpression in the brain tissue after the first injection protocols (1 injection of 1000 µl); also Channelrhodopsin 2 expression was seen in layer IV of the S1;* **B:** *Desired expression areas;* **C:** *Pictures showingexpression limited to only superficial and deep layers of S1 following the second injection protocol (2 injections of 500 µl separated by 1mm posterior to Bregma).*

Signal analysis

To obtain LFPs, signals from the 128 channels on the silicon probe array were bandpassed between 1 and 7500 Hz and continuously recorded at a sampling rate of 30,000 Hz. For the LFP analyses the raw LFP data was further digitally low-pass filtered was by a Butterworth 500 Hz low-pass filter in order to remove the high-frequency signal and to isolate the LFPs, and down-sampled to 2,000 Hz (*Fig. 9*). All LFP analyses were performed on this down-sampled version. For the LFP analysis, we employed custom software developed in MATLAB (*R2016b, http://www.mathworks.com/, Natick, MA, USA*). In parallel, time points (timestamps) for each data point of stimulation were recorded and plotted using custom made MATLAB software. As is the case with high density recording electrodes, it is common for signals that originate from other sources other than the brain region of interest to interfere with the recording and give false positive signals. The sources of these signals can appear either from experimental procedures (electrode position altering, connective wire movement or due subject motion) but also from environmental factors such as electromagnetic (EM) coupling. In this study we experienced a global electric artifact across all channels of the recording probe at the same temporal window (*Fig.9*) due to the a PWM (pulse-width modulation) artifact, created by electromagnetic pulses that occurred when the Arduino switched the stimulation LEDs on and off quickly to regulate average intensity of light. Thus, before analysis of the filtered signal, the stimulus artifacts were removed from the single LFP's traces using a custom algorithm developed in MATLAB. Usually, artifacts have different spatial and temporal characteristics when compared to neural signals, features we used to detect and remove the stimulation artifacts. Local field potentials are most of the time recorded at a frequency between 0,1Hz and 200 Hz with a voltage amplitude of 0,1to 1 mV, while neural spikes are recorded at 300 Hz to approx. 5 kHz with a voltage amplitude of 40 to 500 µV.

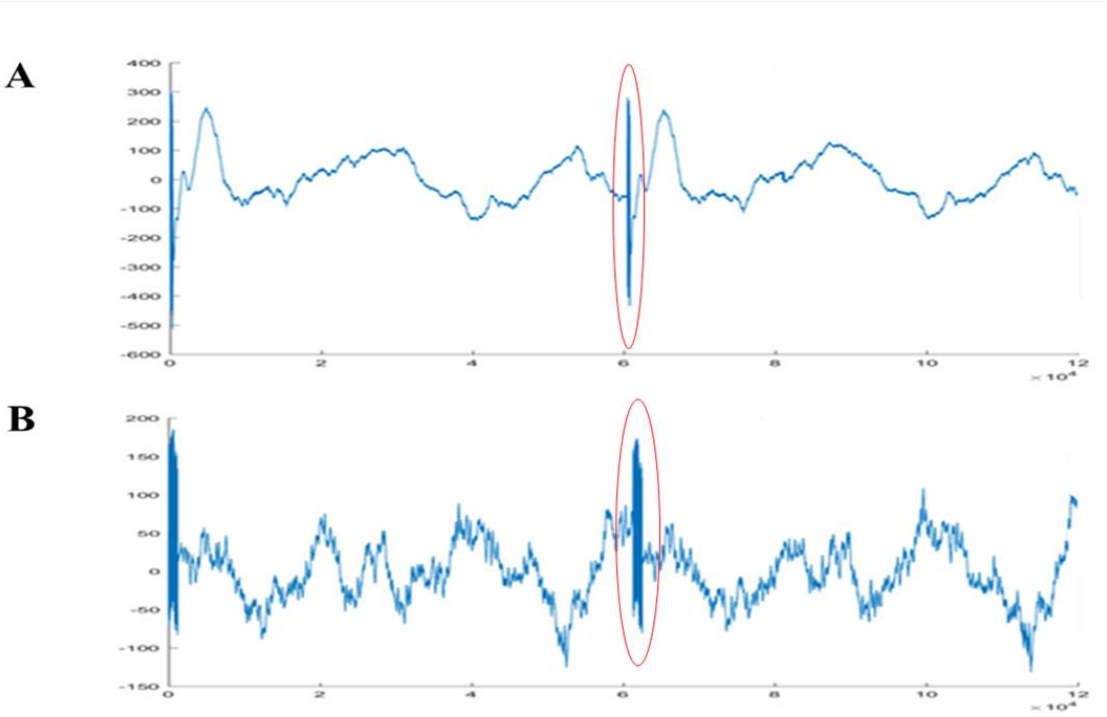

Fig. 9. *Differences between raw data signal traces recorded;* **A:** *and filtered with a Butterworth 500 Hz low-pass filter in order to remove the high-frequency signal and to isolate the LFPs or* **B:** *not filtered signal. Figure shows delineated in red, the spatio-temporal representation of the electric artifacts.*

On the other hand, the electrical and optical stimulation artifacts can be recorded at a frequency between 0 and 10 kHz and with an amplitude of 20mV. Also, the features of the stimulation waveforms are quite stable across recordings and very different than neural signal waveforms. Thus, the artifacts can be removed by digitally detecting the artifact waveforms across all artifacts, and then subtracting the resulting template from the recorded waveform at the time of artifact production (*Wichmann et al., 2011*). Therefore, to remove the PWM artifacts from our LED grid data for each light pulse, we developed a custom MATLAB software that detects all PWM peaks and subtracts the mean PWM waveform from the data. After all the stimulation times were found, the software goes through all stimulation pulses, then calculates the average artifact waveforms for current pulses and subtracts the mean waveform from each segment around an artifact. The stimulus artifact is then removed by replacing the sample points at each stimulus artifact event with values interpolated along a straight line, computed from neighboring sample points. After the artifact removal, we compared spatio-temporal features of the stimulus-evoked responses in the overall LFP traces for different stimuli. An evoked potential or evoked response is an electrical potential recorded from the nervous system following presentation of a stimulus, as different from spontaneous potentials as detected by electroencephalography or other electrophysiological recording method. For the LFP analysis only epochs adjacent to the optogenetic stimulation (0.25 sec before and 0.5 sec after the stimulation) were used to characterize signal features from each individual recording channel and brain region. To further describe relevant features of the LFP signal such as the frequency spectrum, voltage amplitude and latency of the evoked responses (*fig. 10*), we developed a MATLAB based software to analyze these features of each single LFP trace. At first, the algorithm finds the timestamps of each stimulation and transforms each timestamp from seconds into samples based on the sampling rate of the recording system. Next, based on the channel order described by the user, the algorithm loops through all the channels, changes the filename on every iteration of the loop and saves the data in a newly formed matrix.

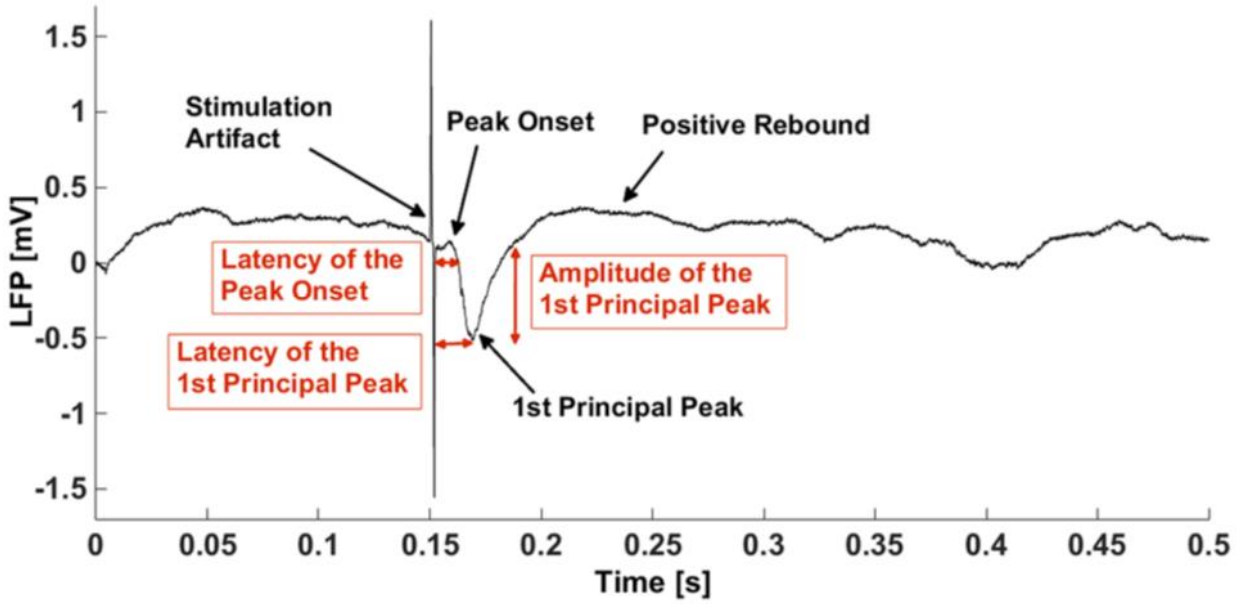

Fig. 10. *Measurement of evoked potential features. Useful features which characterize an evoked response shape include positive and negative gradients, spike width, positive and negative peaks, and peak-to-peak amplitude.*

To cut out the periods we are interested in, we then defined the time in seconds that needs to be analyzed before and after the stimulation timestamps were recorded. The software iterates through all channels and timestamps events and checks whether the periods that were isolated for analysis do not start before the recording starts or are longer than the actual recording. Next, after the start and endpoint of the periods needed for analysis were defined, the algorithm cuts out the periods of interest from the respective channel around the events of interest and subsequently store them in a newly formed 3D matrix. For the next step in the LFP analysis, the raw LFP data was further digitally low-pass filtered by a Butterworth 500 Hz low-pass filter in order to remove the high-frequency signal and down sampled to 2,000 Hz by taking every 15^{th} sample and convert it to a double data format needed for filtering while saving all the data in a new formed 3D matrix. To further visualize and analyze the data, the algorithm next iterates through all the channels again and plots the data in a form of a heat map that represents the actual order of channels in the brain. After that, the software takes the mean over the events for each channel in parallel, and gives out the mean for every channel, which is then squeezed and transformed into a 2D matrix. Measurement of waveform features such as positive and negative gradients, spike width, positive and negative peaks were further used to compare the features of evoked responses for each stimulation condition and each brain region of interest.

The signal features of LFP used to analyze the signal features which include positive and negative gradients, spike width, positive and negative peaks, and peak-to-peak amplitude (*fig. 10)*. The power spectrum was calculated as being proportional to the squared Fourier transform of the data. The Fourier transform is a mathematical formula that relates a signal sampled in time or space to the same signal sampled in frequency. In signal processing, the Fourier transform can reveal important characteristics of a signal, namely, its frequency components. The Discrete Fourier Transform (DFT) is the equivalent of the continuous Fourier Transform for signals known only at $\boldsymbol{N}$ instance followed by the sample times $\boldsymbol{T}$. A common operation in analyzing various kinds of data is to find the discrete Fourier transform (or spectrum) of a list of values. The goal is to pick out components of the data with particular frequencies or ranges of frequencies. We may imagine the Fourier transform as matching the data to sinusoids oscillating at different frequencies. If the data fits the sinusoid pattern, the power at the given frequency is high, while if there is no match between the data and the sinusoid, the power at that frequency is low. We next determined the characteristic features of evoked potentials, such as the voltage amplitude of the signal, frequency spectrum but also measured the latency of evoked potentials when compared to the stimulation time points.

Spike sorting

Most neurons respond to external stimuli by firing action potentials which serve as a means of communication with other neurons. Several devices have been developed for the purpose of recording such events: the stereotrode (*McNaughton 1983),* tetrode (*Reece 1989*), and the MEA, or multi-electrode array (*Thomas 1972*). Analysis of MEA recordings is a technically challenging process because electrodes also record spikes from more than one neuron. The goal of spike sorting is to assign detected spikes to specific neurons, and its reliability depends on the ability to detect and classify spikes. Many spike sorting approaches have been developed, but usually all algorithms are made up of three stages: detecting spikes, extracting spike features and clustering of spikes features. Innovations in electrophysiological methodology, such as high density silicon probes recordings, allow us to monitor in high resolution the activity of large subsets of neurons as well as individual units simultaneously. However, when dealing with such sets of data, mistakes often occur. One of the biggest problems spike detection algorithms face is that temporally overlapping spikes are extremely common. To minimize the effect of this issue, we made use of a three program software suite (Klusta, http://klusta-team.github.io/, *Rossant, C. et al, 2016*), which,

after the spikes are extracted as local spatiotemporal events, are then sorted and attributed to individual neurons using a novel cluster analysis algorithm. One of the basic questions asked in electrophysiology is how to detect a spike. Thus, firstly, we must first understand features of action potentials. One of the most important features is the peak amplitude. When the cell membrane of a neuron is depolarised past its threshold voltage, voltage-gated ion channels open, resulting in an influx of positive ions in the cytoplasm and an action potential. This action potential is recorded and visualized as a spike.

During extracellular recordings, this spike is recorded as a negative peak, since the recording medium is negative with respect to the cell potential. Once the peak amplitude is reached, sodium channels close and potassium channels open, resulting in repolarisation. Repolarisation often occurs past the cell's resting potential, and is seen as a positive peak in extracellular recordings (*fig. 10*). To analyze these spikes, we first needed to filter the raw data signal to remove the slow local field potential signal, given that the neural spikes are recorded at 300 Hz to approx. 5 kHz with a voltage amplitude of 40 to 500 µV. For this step the software implements a 3rd order Butterworth filter used in the forward-backward mode with a band-pass filter of 500 Hz to 0.95*Nyquist (*fig. 11A*). Once the signal is filtered, the first step in detecting action potentials is spike detection and feature extraction (*SpikeDetekt*). *SpikeDetekt* aims at identifying data points which form an action potential. Current spike detection methods make use of prominent features such as the peak amplitude, to enable automatic detection of spikes. The most used technique to address this feature is voltage threshold detection. The voltage threshold method detects data points which lie between a minimum and maximum threshold value (*Lewicki 1998, Zhang 2003, Quiroga 2004, Segev 2004).* In order to discard background noise and detect action potentials only, the voltage threshold must be large enough so as to avoid the detection of background noise. If the spiking neuron is located far away from the electrode, low amplitude spikes may not be detected by the voltage threshold method (*fig. 11B*).

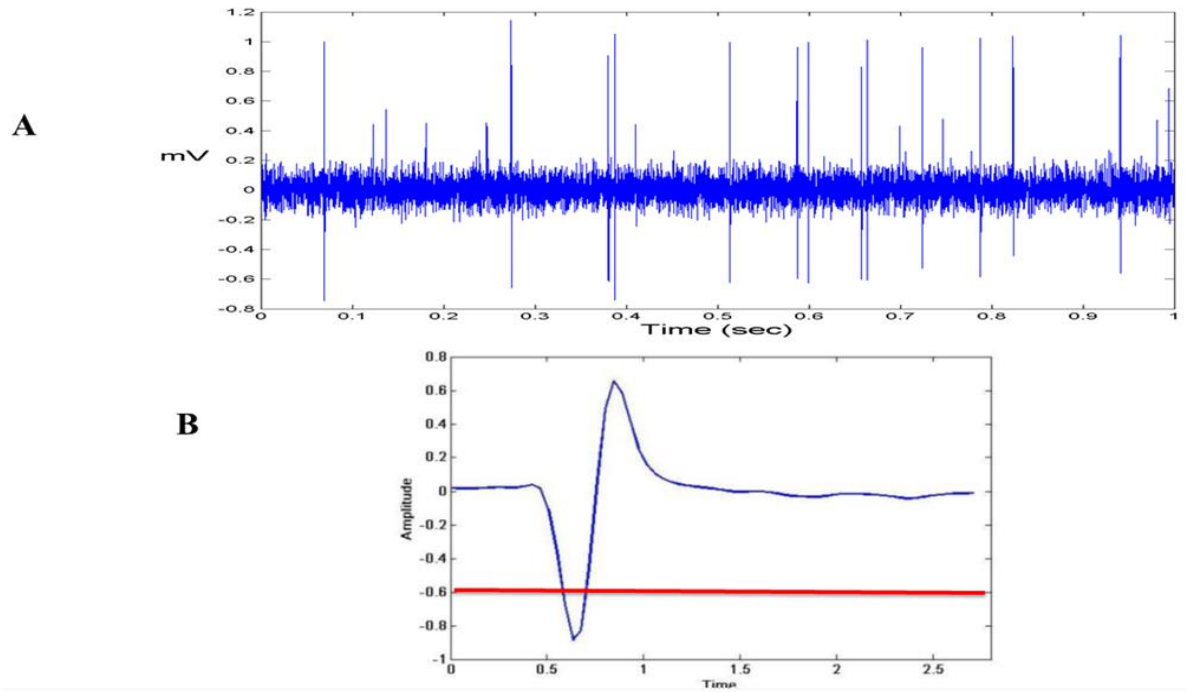

Fig. 11. A: *Figure showing the filtered data using the a 3rd order Butterworth filter used in the forward-backward mode with a band-pass filter of 500 Hz to 0.95*Nyquist; Similar to LFP analysis, we needed to filter the raw data signal to remove the slow local field potential signal, given that the neural spikes are recorded at 300 Hz to approx. 5 kHz with a voltage amplitude of 40 to 500 µV.* **B:** *Example of a voltage gated threshold. The red line indicates the level of the arbitrary chosen value for the minimum threshold.*

The spike detection module detects action potentials as spatiotemporally localized events based on two thresholds: the strong threshold is found at 4 times the standard deviation (SD) of the filtered signal, while the weak threshold is set at 2 times the SD and a power weight of 2. The standard deviation is computed with a robust estimator, median ($|V|$)/.6745, to avoid contamination by spike waveforms. For a positive identification of a spike, the filtered signal needs to exceed the weak threshold for every point, and at least one point needs to exceed the strong threshold. In this way the dual-threshold approach limits the detection of small noise events, which may be interpreted as neural spikes. After the spikes are detected using the double threshold algorithm, spikes must be temporally aligned before sorting. This represents a critical step in spike sorting algorithm because usually, spikes from a single neuron that are misaligned could be taken into consideration as spikes from multiple neurons. To avoid this, the *SpikeDetekt* software is assigning each spike a central time given by the center of mass of the spike's supra-threshold components, weighted by a power parameter.

The next step in the *SpikeDetekt* software after spike detection is feature extraction. Neurons typically produce spikes with a characteristic shape (*Lewicki 1998*). If we assume that a neuron's spike shape does not change in time, we can characterize its shape by extracting spike features. Overlapping spikes may also be recorded when two or more action potentials reach an electrode at the same time. A simple method of analyzing spike shapes is through the direct measurement of spike features such as the peak-to-peak voltage amplitude, spike width, and spike gradient (*Fig. 10*). Spike features can be used to discriminate between spikes from different neurons. This method may be used on a single electrode or across multiple electrodes. *Figure 13 Right Up* shows a scatter plot of peak amplitudes recorded on 2 neighboring electrodes. There is a clear clustering of two different spike shapes indicating that the detected spikes originated from two different neurons. After that, based on the geometry of the probe which is specified by the user using an adjacent graph (*Rossant C. et al., 2016*), a spatial component is added to the analysis to accurately describe the spatiotemporal characteristics of each waveform. Subsequently, every waveform is realigned around their central time and summarized compactly by two vectors, referred to as the "feature vector" and the "mask vector" (*Fig.12*). The feature vector is found by applying principal component analysis (PCA) to the aligned waveforms on each channel (3 principal components were kept for the current analysis). PCA is commonly used statistical method to automatically extract spike features for spike classification (*Lewicki 1998, Zhang 2003*). The aim of PCA is to compute an ordered set of orthogonal basis vectors which can be linearly combined to describe each detected spike. This method assumes that the largest variation in a set of data contains the dynamics of interest (*Lewicki 1998, Shlens 2005*). All channels are used in computing the feature vector while the mask vector is computed from the peak spike amplitude on each detected channel. The mask vector allows temporally overlapping spikes to be clustered as separate cells (*Fig.12*). Because temporally overlapping spikes have similar feature vectors, further information such as the mask vectors must be used to distinguish these spikes, which will be used in the second step of the spike sorting algorithm, *KlustaKwik*. KlustaKwik automatically determines the number of clusters that best fit the data, in which different points are defined by a different subset of relevant dimensions such as peak-to-peak voltage amplitude, spike width, and spike gradient analysis calculated for each point of data. Since fully automated software analysis showed more consistency and lower error rates than fully manual spike sorting, automatic analysis cannot be fully trusted to accurately classify all spikes, and manual verification is a must (*Rossant C. et al., 2016*). The final step of the spike sorting pipeline is manual verification and correction of cluster assignments, which are implemented in the program *KlustaViewa.*

The usual manual corrections consists of merging clusters corresponding to a single neuron that were not joined by the automatic algorithm. Errors in splitting a single neuron's spike waveforms to different locations often occur due, mainly to, electrode drift and cell bursting, however, these waveform

shifts can be identified by manual inspection of waveforms, auto- and cross-correlograms, and cluster shapes. The software iterates through all clusters starting with the best currently unsorted spikes while the remaining clusters are ordered by similarity to the best unsorted cluster. The decision of whether to merge, split, or delete each merge candidate is in the end made by the operator (*fig. 13 Left side*). The manual stage was designed to present the operator with decisions that can be made quickly, with the most important decisions presented first. The similarity matrix presented in the software interface helps guide the operator to cluster remaining data points attributed to different waveforms, and thus, based on the principal component analysis, to accurately assign each data point to its corresponding waveform (*fig. 13 Right up*). The auto-correlograms of all recorded spike trains, were calculated for ±500 ms offset with bin size of 1 ms. The power spectra of the spike trains were calculated by the Fourier transform of the autocorrelograms, allowing 1 Hz resolution of the frequencies. The power spectra was calculated after removing the trough of the refractory period around time 0 in the autocorrelograms (reducing high-frequency noise) and after subtracting the average firing rate of the cell (*fig. 13 Right down*).

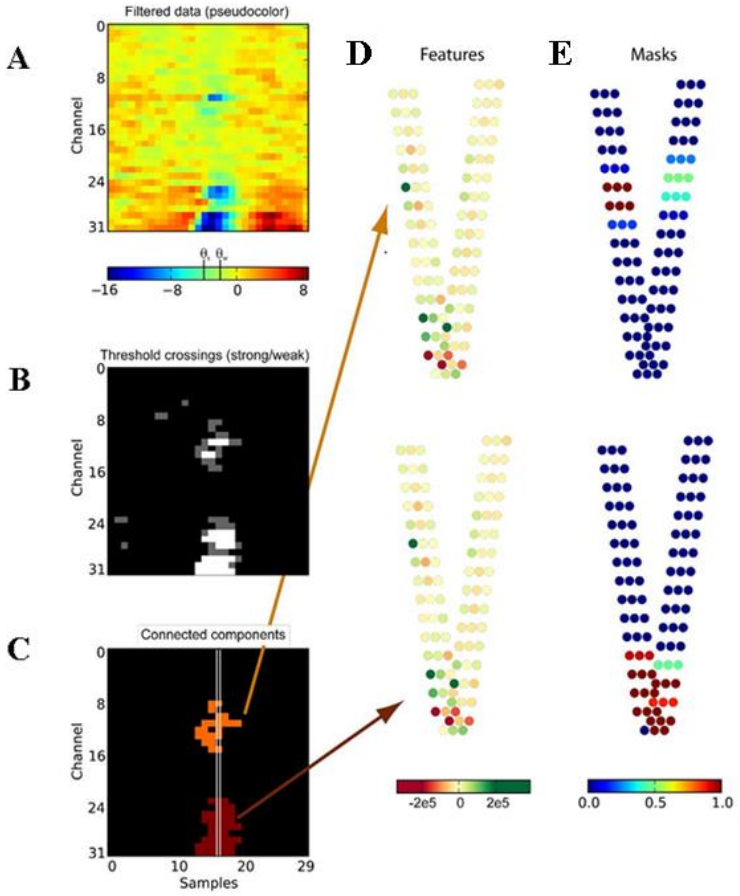

Fig 12. A: *High-pass filtered data. Vertical lines on the color bar indicate strong and weak thresholds, (respectively 4 and 2 times standard deviation).* **B:** *Gray-scale representation showing samples which cross the weak threshold (gray), and the strong threshold (white).* **C:** *Results of two-threshold flood fill algorithm, showing connected components corresponding to the two spikes in orange and brown. White lines indicate alignment times of the two spikes.* **D:** *Pseudocolor representation of feature vectors for the two detected spikes (top and bottom). Each set of three dots represents three principal components computed for the corresponding channel. Note the similarity of the feature vectors for these two simultaneous spikes (top and bottom).* **E:** *Mask vectors obtained for the two detected spikes (top and bottom). Unlike the feature vectors, the mask vectors for the two spikes differ. Each set of three dots represents the three identical components of the mask vector for the corresponding channel as described by Rossant C. et al., 2016.*

As mentioned above, most errors in the spike sorting pipeline are due to the fact that merging clusters corresponding to a single neuron were not joined by the automatic algorithm. However, at this stage of spike sorting, other issues might occur. Two different waveforms, corresponding to two different cluster locations can be identified and grouped as a single waveform attributed to only one cluster (*fig. 14A*). For this, we made use of the similarity matrix provided by the software interface. Here, based on the PCA analysis, data points are clustered around a particular orthogonal dimension, which allows the user to easily have access to data points that are exceeding the deviation. Visually, we can identify these data points in the similarity matrix as points farther away from the center of the orthogonal dimensions. By selecting these data points, they are assigned to a newly formed cluster. The new cluster is then undergoing iterations through all clusters starting with the best currently unsorted spikes and based on its waveform is attributed to an already existing cluster or a new one is created. To correctly assign these new formed clusters to already established ones, we made use of the auto- and cross-correlograms. Here, based on waveform similarities, we compared each new cluster to an already created one based on their specific refractory period. The classification of these new clusters was estimated using the cross-correlograms on pairs of recorded units. After the manual verification and validation of automatic merged clusters, we next assigned each individual cluster to its corresponding neuron. For every neuron we then plotted raster plots of generated and sorted spikes using a custom made MATLAB software (*fig. 14B*).

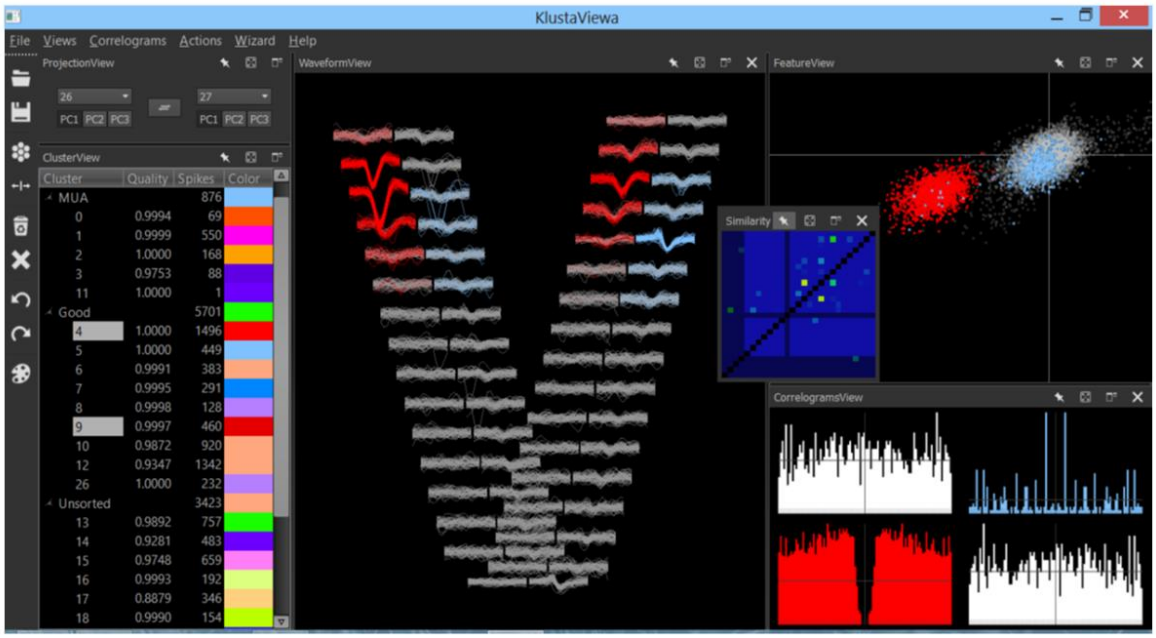

Fig. 13. *Screenshot of the KlustaViewa graphical user interface as described by Rossant C. et al., 2016.* ***Left:*** *clusters are ordered by similarity to the best unsorted cluster, and the decision of whether to merge, split, or delete each candidate is made by the operator;* ***Center:*** *spatial and temporal characteristics of the evoked responses waveforms of each individual recording channel based on the silicon probe architecture;* ***Right up:*** *the similarity matrix presented in the software interface helps guide the operator to cluster remaining data points attributed to different waveforms based on the principal component analysis;* ***Right down:*** *the auto- and cross-correlograms of two recorded spike trains, calculated for ±500 msec offset with bin size of 1 msec.*

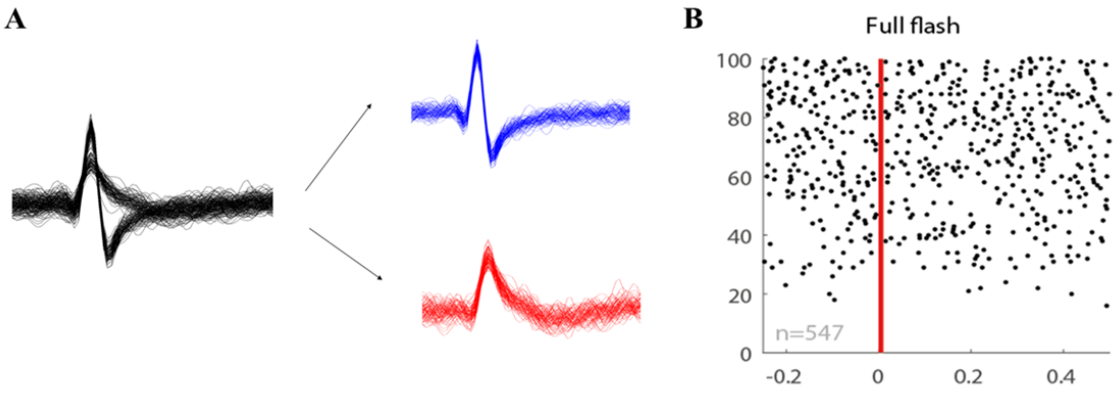

Fig. 14. A: *Example of two different waveforms identified and grouped together as a single waveform;* **B:** *Example of a raster plot for the activity of a single neuron.*

Results

Immunohistochemistry and viral tracing

To accurately identify the downstream cortical and subcortical brain targets which receive input projections from the rat supra- and infra-granular layers of S1, we have examined the distribution of anterogradely labeled axons arising from viral tracer (AAV5-adenoassociated virus) injections in layers V and VI of S1, through analysis of section images from three experiments.

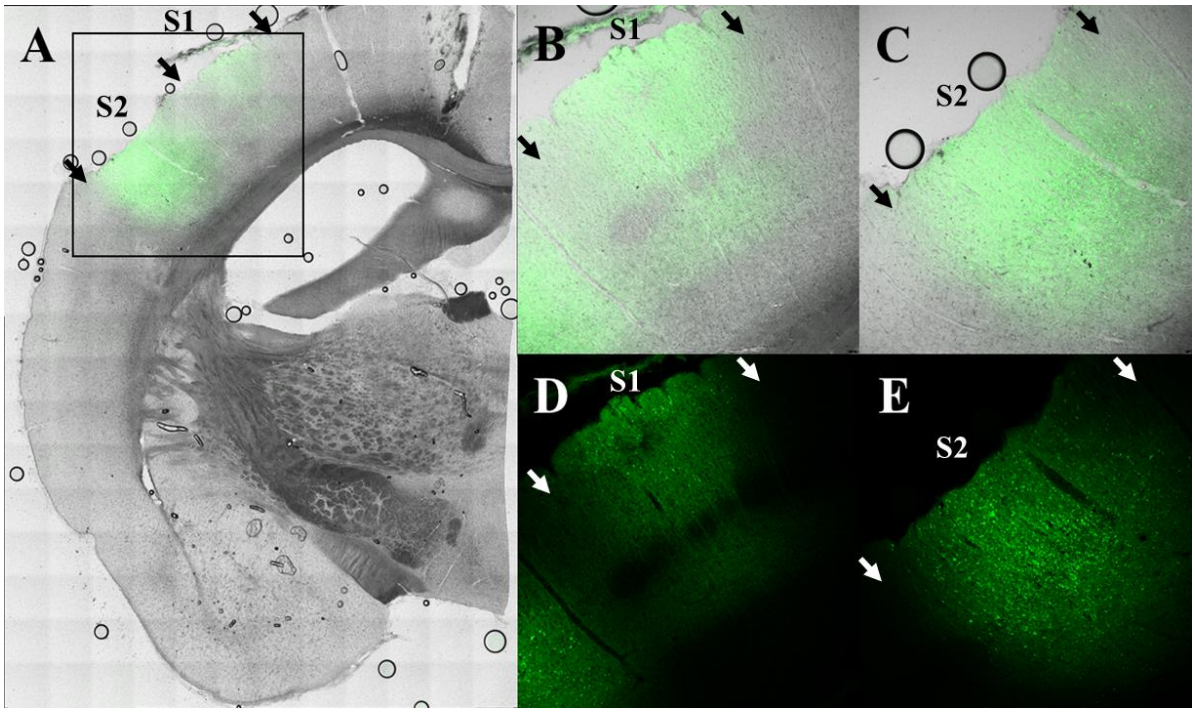

Fig. 15. A: *Confocal microscopy image showing the localization of the AAV5-GFP opsin expression after injection of the viral construct in layers V and VI of the S1. Note that the viral expression was limited to only the infra- and supra-granular layers of S1.* **B, C:** *Confocal microscopy images showing the viral expression of GFP over the S1 and respectively S2.* **D, E:** *Fluorescence microscopy images showing the viral expression of GFP over the S1 and respectively S2. Black arrows represent the anatomical boundaries of S1 and S2; Paxinos and Watson, 2007.*

The two sets of injections for each of the three animals used for this experiment (*see Surgery – viral vector injection*) did not vary in volume and covered the entire thickness of the cerebral cortex surrounding the BF of the rat S1 without the involvement of the layer IV (cellular aggregates which constitute the whisker representation, also known as barrels) and showed sharp boundaries (*fig 15 A, B, D*). The position of the injection sites were determined from histological analyses of anatomical features and cytoarchitectural patterns. The shape and density of labeled fibers were similar across experiments. Since bilateral projections were observed, the contralateral staining was lower when compared to the ipsilateral labelling, however, it followed the same pattern as ipsilateral projections. All viral tracer injections gave rise to labeled axons in most parts of the injected S1 cortex, apart from the barrel granular layer, thus highlighting the intricate pattern of connectivity within the S1 network (*Fabri and Burton, 1991a, Feldmeyer et al., 2013*). We observed ample amounts of labelling in the ipsilateral S2 (*fig 15 A, C, E*), contralateral S1 cortex (*fig. 16 C*), but also extended to subcortical targets such as the ipsilateral dorsal striatum (*fig 16 A, B*). These cortico-cortical and cortico-striatal projections are well described by previous studies (*Brown et al., 1998; Alloway et al., 1999; Hoffer and Alloway, 2001*) and in accordance to these experiments we describe a dense and prolonged clusters of labelled axon fibers arising from layers V and VI of S1 to ipsilateral and, in smaller amounts, to the contralateral dorsal striatum.

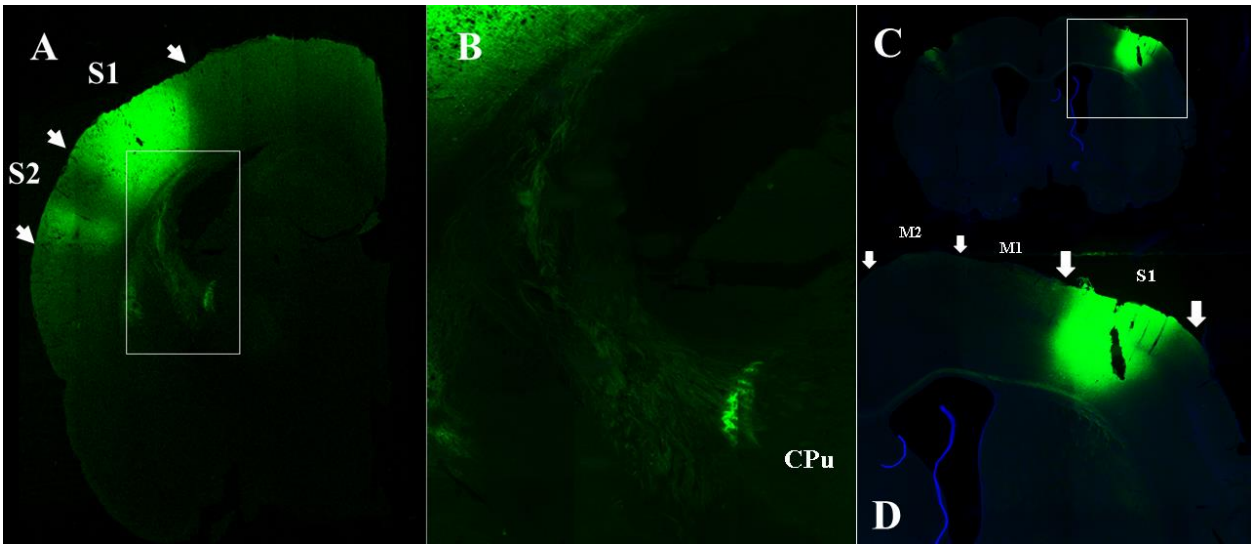

Fig. 16. A: *Fluorescence microscopy image showing AAV-GFP expression in S1, S2 and labelled fibers projecting to the dorsal striatum CPu (Caudate-Putamen);* **B:** *Enlarged image of the highlighted area in Fig. A showing labelled fibers projecting to the dorsal striatum;* **C:** *Image showing AAV-GFP labelling of fibers in the contralateral S1;* **D:** *Enlarged image of the highlighted area in Fig. C showing AAV-GFP labelling in S1 as well as labelled fibers protruding from layers II-III and V-VI of S1 towards M1 and M2. Note the ordered pattern of projections from deep and superficial layers towards M1 and M2; M1, M2 – primary and secondary motor cortex, S1,S2 – primary and secondary somatosensory cortex. White arrows indicate the anatomical boundaries of S1, S2, M1, M2; Paxinos and Watson, 2007.*

Anterogradely labelled fibers stemming from S1 were also seen in motor cortex (M1 and M2), and these labelled areas maintain a relative clear spatial order in correspondence to S1layer specific input (*fig. 16 D*). The area described here as M2 based on the *2007 Paxinos and Watson* rat brain atlas includes the medial and lateral agranular cortex and the labelling observed in this study fits rather well with previous research on S1 projections, in which that the labelled axons from S1 were seen to be distributed across the transition zone between the medial and lateral agranular cortex (AGm, AGl respectively) (*fig. 17 A1-4*) (*Smith and Alloway, 2013; Zakiewicz et al., 2014*). This arrangement is maintained throughout the posterior – anterior axis but surprisingly not in its entirety. As we moved further along the posterior – anterior axis, the resulting arrangement of labelled fibers moved from the border between AGm and AGl to a more widespread layout covering in large amount the dorsal area of M2, making the transition area between AGm and AGl not recognizable anymore (*fig. 17 A4*).

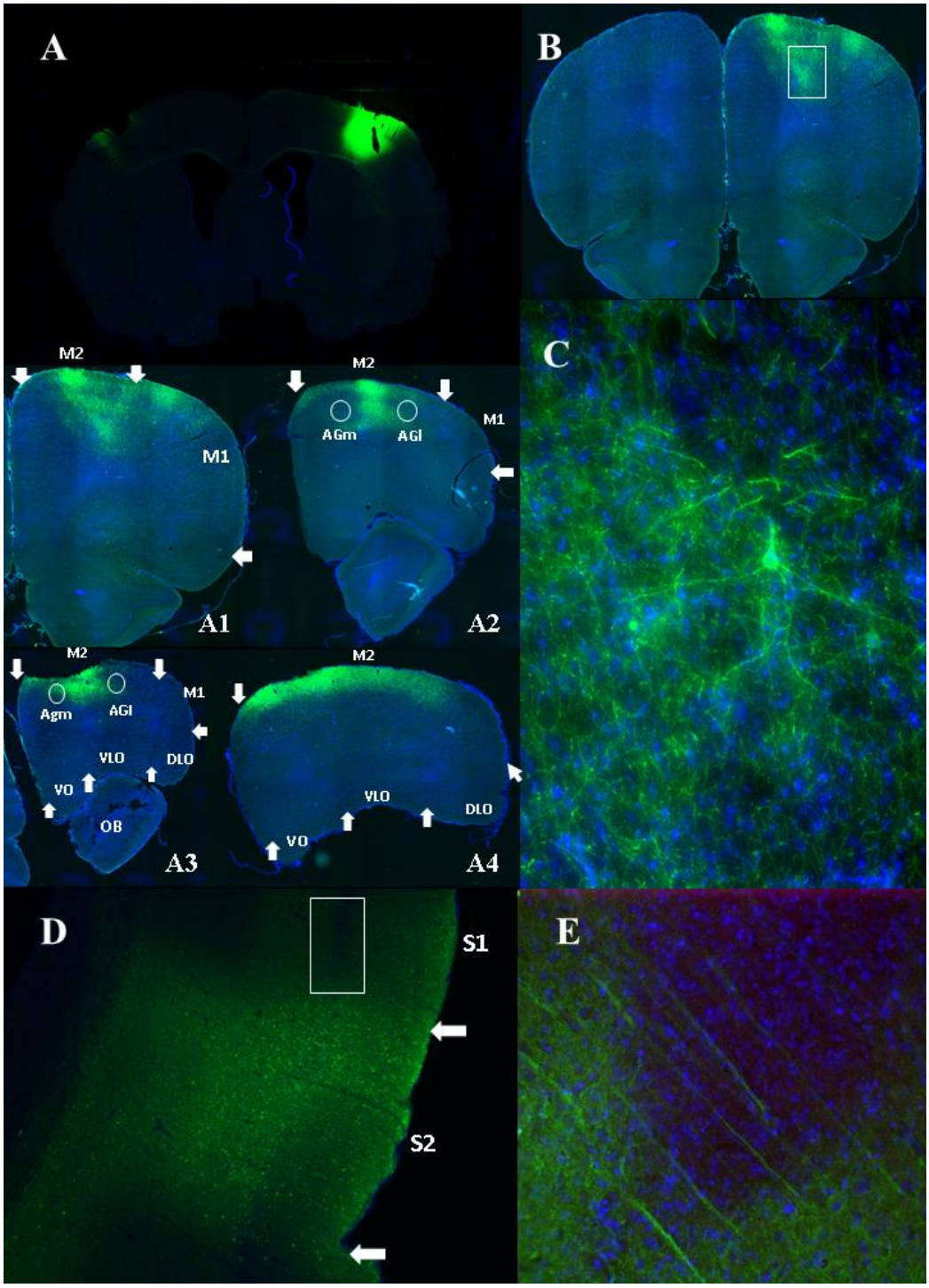

Fig 17. A: *Fluorescence microscopy image showing the spread of the viral construct across hemispheres;* **A1:** *Image showing the spread of labelled axons spread across the M1, M2 – Bregma + 3.7mm;* **A2:** *Image showing the spread of labelled axons spread across the M1, M2 – Bregma + 4.2 mm;* **A3:** *Image showing the spread of labelled axons spread across the M1, M2 – Bregma + 4.6 mm;* **A4:** *Image showing the spread of labelled axons spread across the M2 – Bregma + 5.1 mm;* **B:** *Image showing ipsilateral but not contralateral labelling areas in M1 and M2;* **C:** *Enlarged image showing the highlighted area in Fig.C;* **D:** *Image showing viral expression patterns in S1 and S2;* **E:** *Enlarged image showing the highlighted area in Fig. D – cellular aggregates (barrels) stained in blue (DAPI); Paxinos and Watson, 2007. White arrows indicate the anatomical boundaries of S1, S2, M1, M2, OFC subdivisions.*

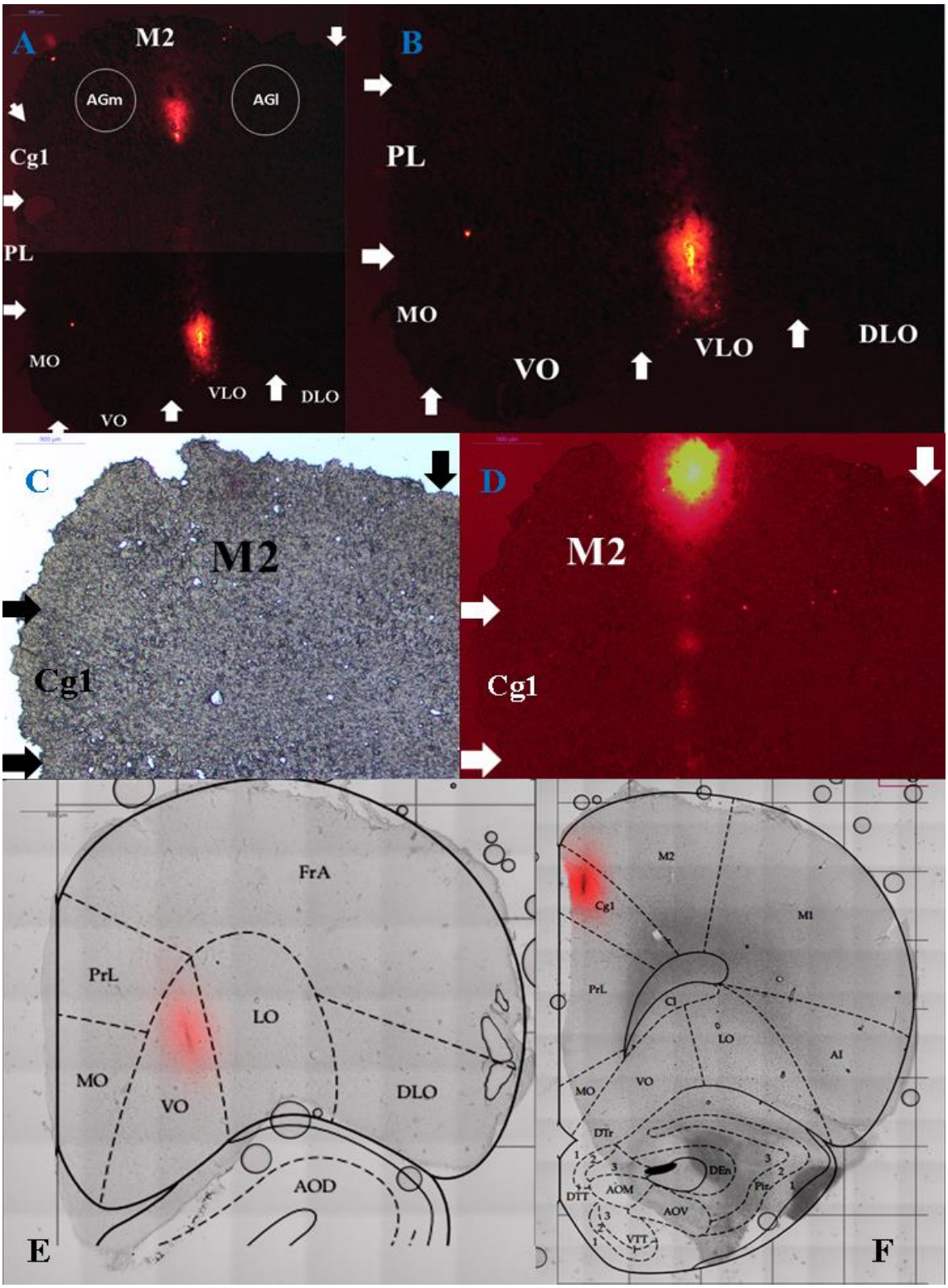

Fig. 18. A: *Fluorescence microscopy image showing the position of the silicon probe in the PFC;* **B:** *Enlarged image showing the silicon probe placement in the OFC;* **C:** *Bright field microscopy showing the medial part of the PFC;* **D:** *Fluorescence microscopy showing the silicon probe tract in M2;* **E, F:** *Confocal images showing the silicon probe tracts in OFC and M2/Cg1.*

Despite previous studies which showed anatomical projections from S1 to ipsilateral OFC in mice (*Mao et al. 2011; Aronoff et al. 2010*) but also in rats (*Bedwell et al.2014*), in this study we haven't identified a direct projection from supra- and infra-granular layers of S1 to the OFC, which is agreement with other previous data which also failed to uncover a direct anatomical link between these two brain areas (*Zakiewicz et al.2014*) nor a functional relationship (*Golmayo et al. 2003*) (*fig 17 A2-4*). Due to the narrow shank of the silicon probe, coupled with the fact that the electrical properties of these high density probes do not allow for flux of current in order to scar the tissue after the experiments, getting an accurate assessment of the probe localization proved to be impossible. To address this problem, before the silicon probe was lowered in the desired cortical position, a lipophilic dye (DiL) was used to coat the shank of the probe. In this way, with the aid of fluorescent and confocal microscopy, we were able to accurately localize the probe placement after subsequent immunohistochemistry (*fig.18*). All probe recordings that were not in the desired locations for this study (*fig. 18 F*) were discarded from the subsequent analysis.

Electrophysiology

The effect of the optogenetic stimulation of S1 on the activity of prefrontal downstream targets (M2 and OFC) was assessed by comparing the main features of the evoked single LFPs recorded in different cortical layers and brain regions from two animals, but also the activity of individual cells. Due to the distribution of the recording channels on the shank of the silicon probe, which allowed us to monitor the activity of large sets of neurons across cortical layers, the results obtained from the main features of the evoked responses show a degree of variability of the LFP across cortical layers and brain regions. This variability is mostly associated with increases or decreases in the amplitude of the evoked responses but not with the onset of LFPs. Optogenetic excitation of supra- and infra-granular layers of S1 cortex induced evoked responses in the superficial and deep layers of M2 at different locations across the anterior-posterior axis (Bregma + 3.7 mm to + 4.3 mm) but also across the dorsal-ventral axis (0 = cortex surface, -0.6 to -1.4) (*fig. 19, 20*) (paired Ttest, $p = 7.999e\text{-}19$ for DV +1.5 and $p = 1.1735e\text{-}19$ for +1.7 DV probe coordinates). Statistical significance was achieved when comparing average LFP epochs before and after the stimulation protocol (0.25 msec. before and after stimulation) on the same location and recording site to provide comparison between baseline recordings and stimulation protocol. For this we compared the amplitude of the first principal peak and the amplitude of the positive rebound phase (*fig. 10*) before and after optogenetic stimulation for the averaged LFP evoked responses (*fig. 19, 20 and 21*) and only the amplitude of the first principal peak and positive rebound phase after the optogenetic stimulation (*fig. 19 B, 20 B, 21 B,*). Significant *p* levels were considered only if they reached the values lower than *0.05*. This was in agreement with the histological analysis which showed a distribution of labeled fibers stemming from S1 all across the superficial and deep layers of M2 (*fig. 17 A1-A4*). However, the optogenetic stimulation of S1 did not induce any significant evoked responses in either deep nor superficial layers of the subdivisions of the OFC (Bregma +3.7 mm to + 4.3 mm) (Paired Ttest, $p = 0.707$) (*fig. 21*), which mirrors the histological analysis, in which no labeled fibers stemming from S1 were seen in the OFC subdivisions (*fig. 17 A1-A4*). However, it is fair to mention that after preliminary analysis showed evoked responses in the deep layers of OFC, but since they appeared before the stimulation protocol, we considered that the responses were not due to the optogenetic stimulation of S1. The distribution of the amplitude of the LFPs varied between cortical layers and was very dependent on the silicon probe location at the time of recording. Given the distribution of labeled areas across cortical layers, the evoked responses showed an increase in amplitude when the shank of the probe was closer to labeled areas when compared to areas in M2 that did not show any labeling (*fig. 19, 20, 21*).

Next we addressed the issue of whether the evoked responses recorded were in fact due to the optogenetic stimulation. For that, we compared LFP traces recorded from animals which had GFP expression in S1 with LFP traces recorded from control animals which did not have S1 GFP expression, in M2 and OFC cortices. Interestingly, the results showed a significant increase (paired Ttest, $p = 4.899e\text{-}19$ for DV +1.5 and $p = 1.0035e\text{-}19$ for +1.7 DV probe coordinates) in the amplitude of the evoked responses

across the M2 area of GFP expressing animals when compared with controls, for the same location and recording site, albeit differences in amplitude of such evoked responses can be also attributed to the proximity of the silicon probe to the GFP labelled areas (*fig. 22 A, B*). In this case, statistical significance was achieved by comparing the LFP epochs (250 msec. after optogenetic stimulation) from each brain between experimental animals and control. However, the recordings were performed to a certain degree, in the same cortical coordinates, thus reinforcing the evidence that the evoked responses recorded in the M2 area were in fact due to the optogenetic stimulation protocol (*fig. 22 B*).

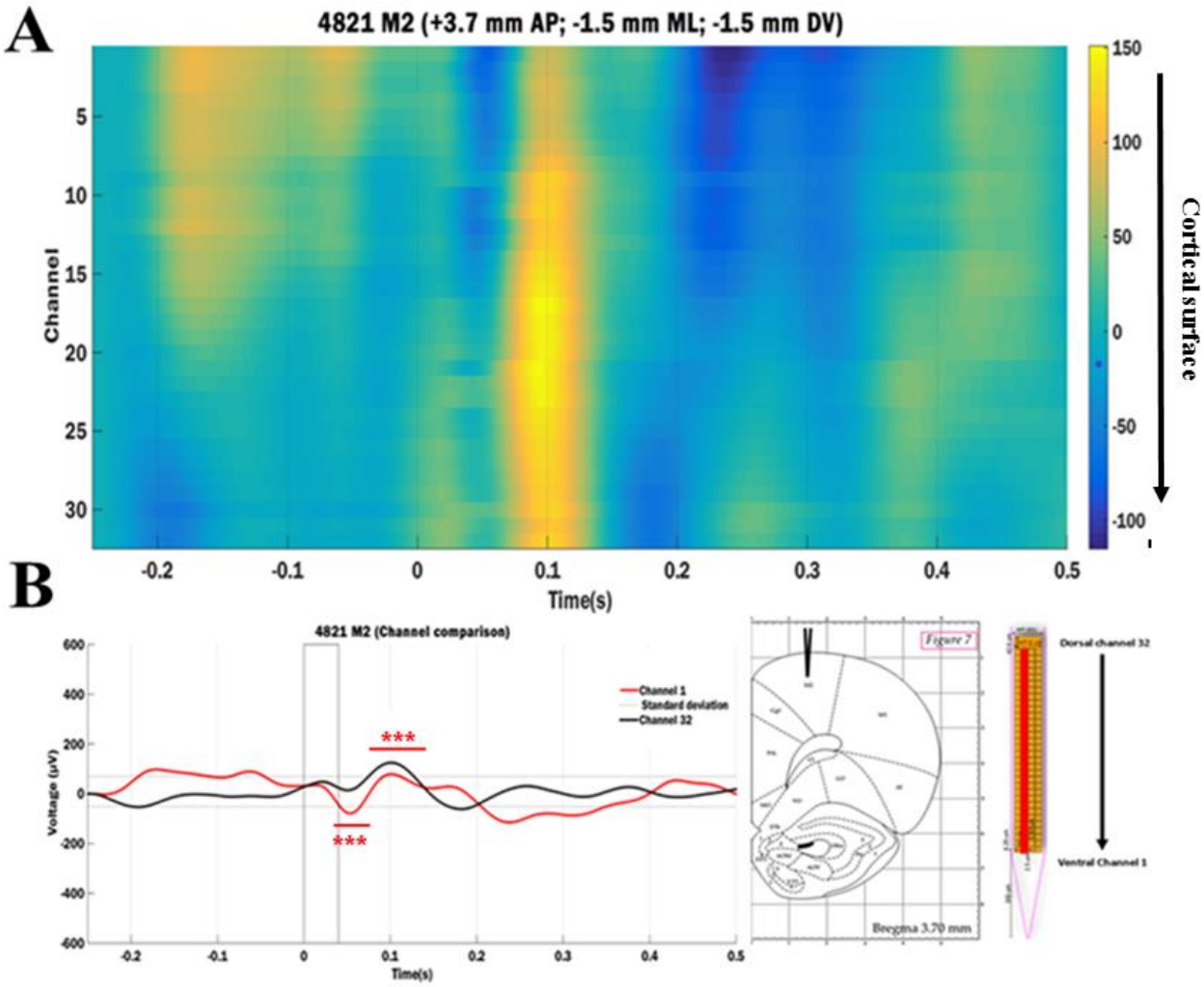

Fig. 19. A: *Heat map plot showing the channel average in voltage across 32 channels, recorded in the M2 (-1.5 DV mm from cortical surface) area, before and after the stimulation protocol;* **B:** *Comparison between the most ventral and dorsal channel on the silicon shank which shows variability in the amplitude of the signal in the DV axis; Black rectangle signifies the stimulation period (40 ms). On the right side, a graphic illustration showing the depth of the recording site and the channel order used in the analysis; Paxinos and Watson, 2007. *** significance of p < 0.01 (paired T test).*

Moreover, when LFP traces recorded from GFP expressing animals were compared with those of control animals in the OFC areas, no significant increase (paired Ttest, $p = 0.673$) in the amplitude of the evoked responses was shown between experimental animals and controls. This was in agreement with the histological data that showed no labeled fibers stemming from S1 to the OFC, in which case no significant differences between the amplitudes of LFP traces due to the optogenetic stimulation could have been

recorded (*fig. 17 A1-A4, 21, 22 C*). This pattern also fits the electrophysiology results from animals who do show GFP expression in M2 but not OFC (*fig. 19, 20*), in which case evoked responses could be recorded in M2 but not OFC. To furthermore investigate the functional relationship between the S1 and OFC, we compared the individual cell activity before and after the stimulation protocol in M2 and OFC areas. Keeping in line with previous results from the LFP analysis, no significant changes in the firing patterns of individual neurons was observed in the OFC (*fig. 23*). Although we recorded the activity of approx. 300 or more cells in each animal, the fact that no significant changes in the firing rate of these neurons due to S1 stimulation, when compared to the baseline, were seen, just strengthen the hypothesis that, at least in rats, there is no functional connectivity between the supra- and infra-granular layers S1 and the OFC subdivisions.

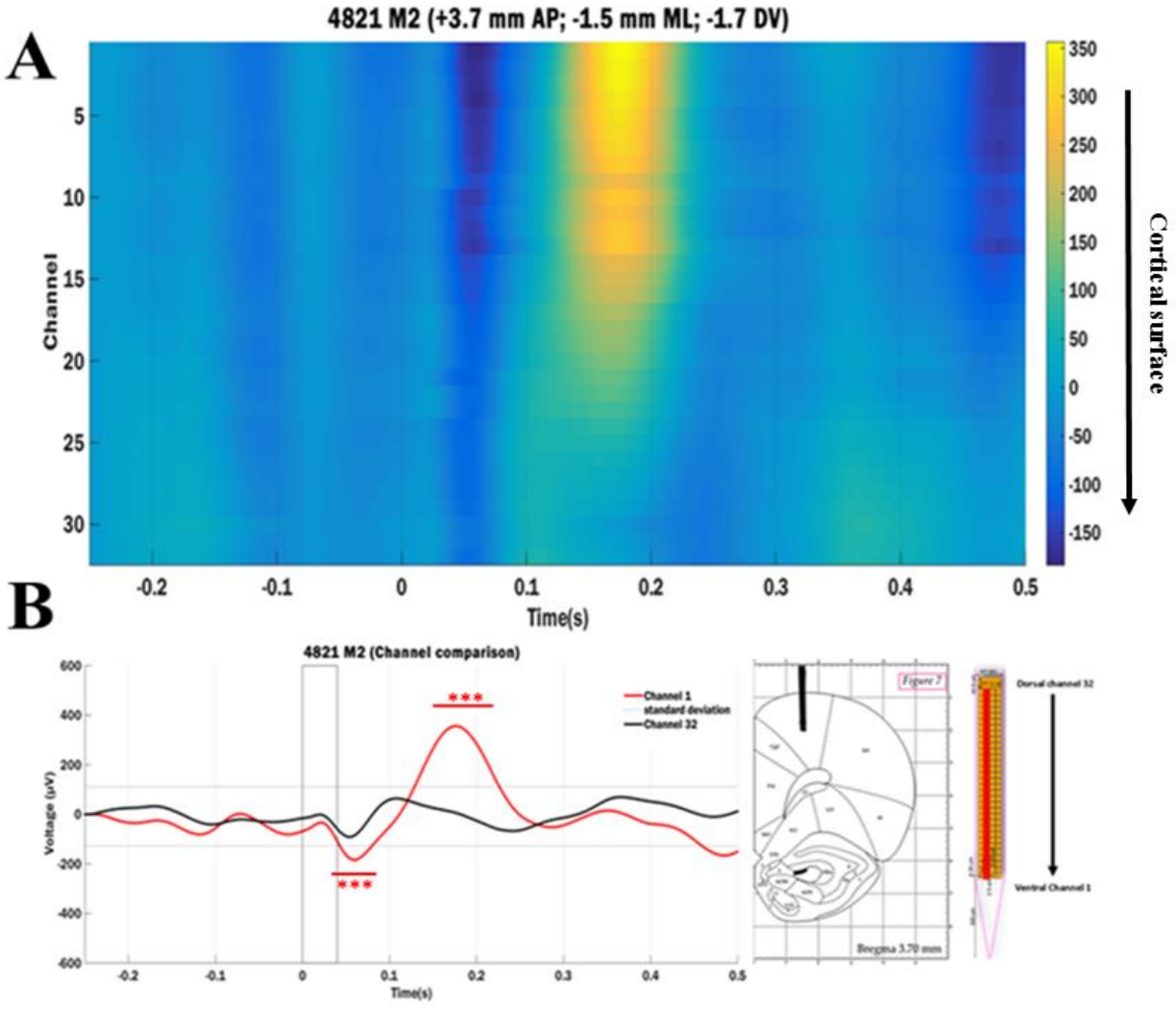

Fig. 20. A: *Heat map plot showing the channel average in voltage across 32 channels, recorded in the M2 (-1.7 DV mm from cortical surface) area, before and after the stimulation protocol;* **B:** *Comparison between the most ventral and dorsal channel on the silicon shank which shows variability in the amplitude of the signal in the DV axis; Black rectangle signifies the stimulation period (40 ms). On the right side, a graphic illustration showing the depth of the recording site and the channel order used in the analysis; Paxinos and Watson, 2007. *** significance of p < 0.01 (paired T test).*

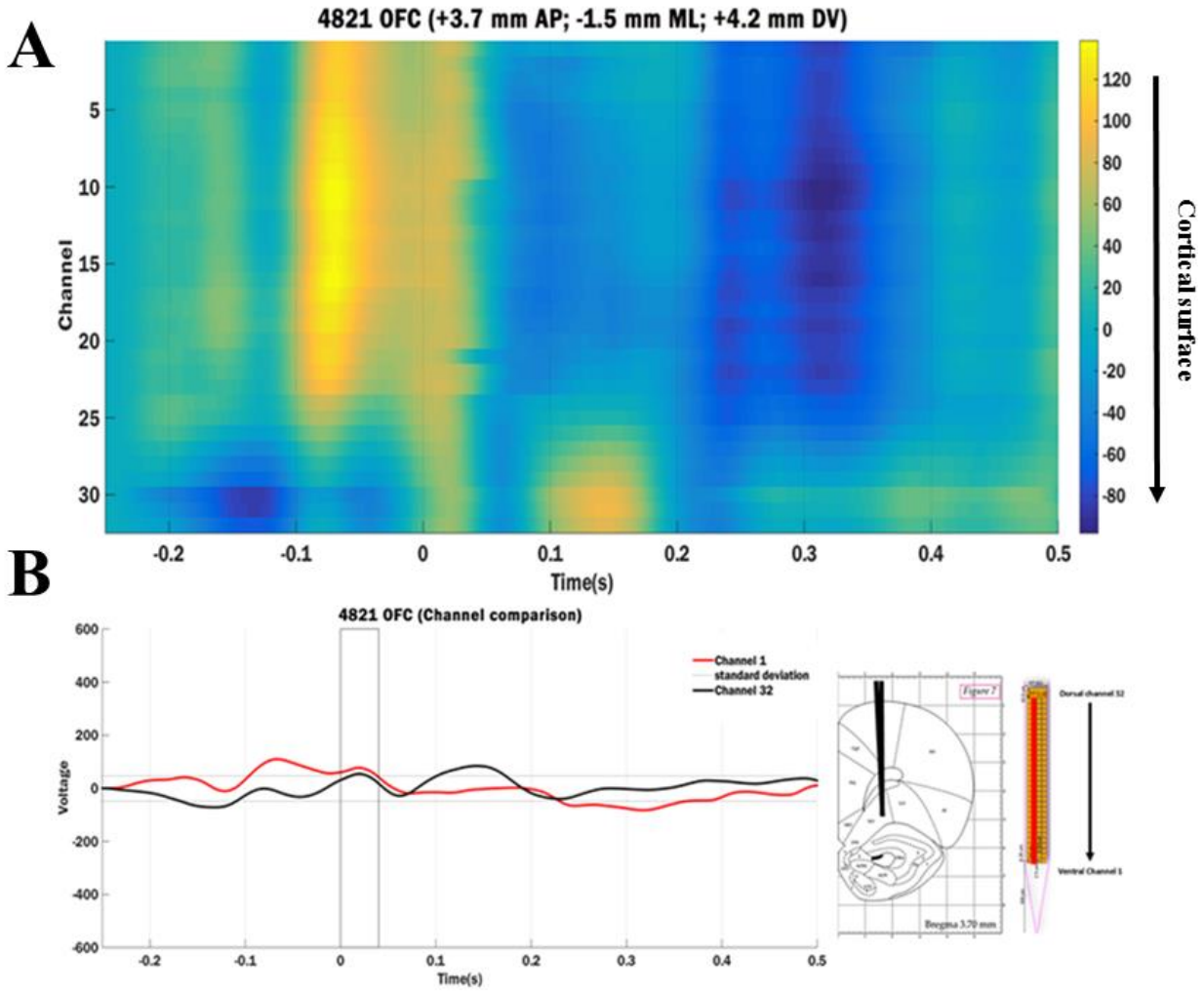

Fig. 21. A: *Heat map plot showing the channel average in voltage across 32 channels recorded in the OFC (-4.2 DV from cortical surface) before and after the stimulation protocol;* **B:** *Comparison between the most ventral and dorsal channel on the silicon shank which shows variability in the amplitude of the signal in the DV axis; Black rectangle signifies the stimulation period (40 ms). On the right side, a graphic illustration showing the depth of the recording site and the channel order used in the analysis; Paxinos and Watson, 2007.*

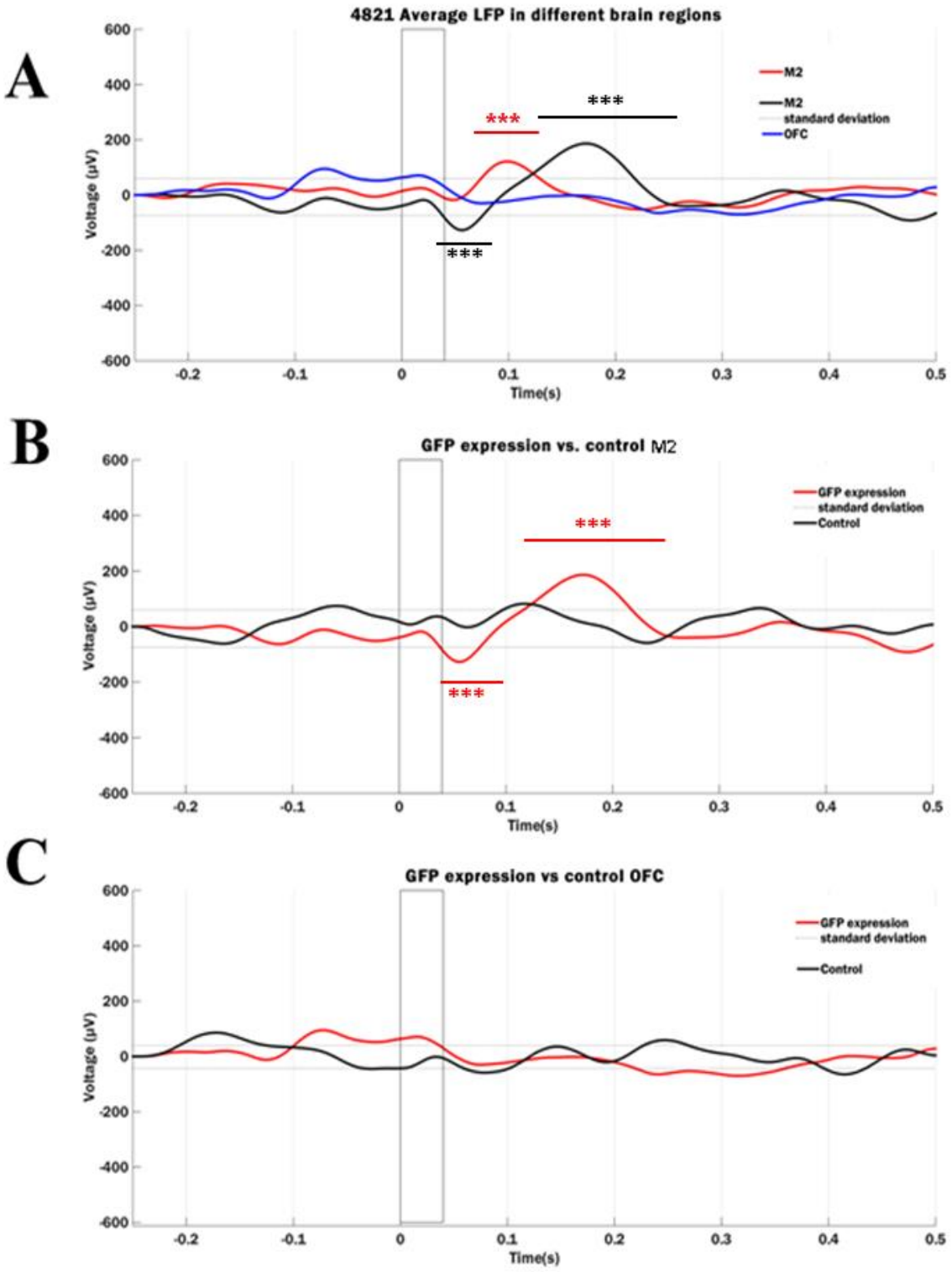

Fig. 22. A: *Graph showing the mean average of the LFP taken over 32 channels in M2 and OFC following optogenetic stimulation of S1 for the same animal;* **B:** *Graph showing the mean average in LFP during the stimulation protocol between GFP expressing animals in S1 vs. controls (no GFP expression in S1) in the M2 area;* **C:** *Graph showing the mean average in LFP during stimulation protocol between GFP expressing animals and controls in OFC area. Black rectangle signifies the stimulation period (40 ms); *** significance of p <0.01 (paired T test).*

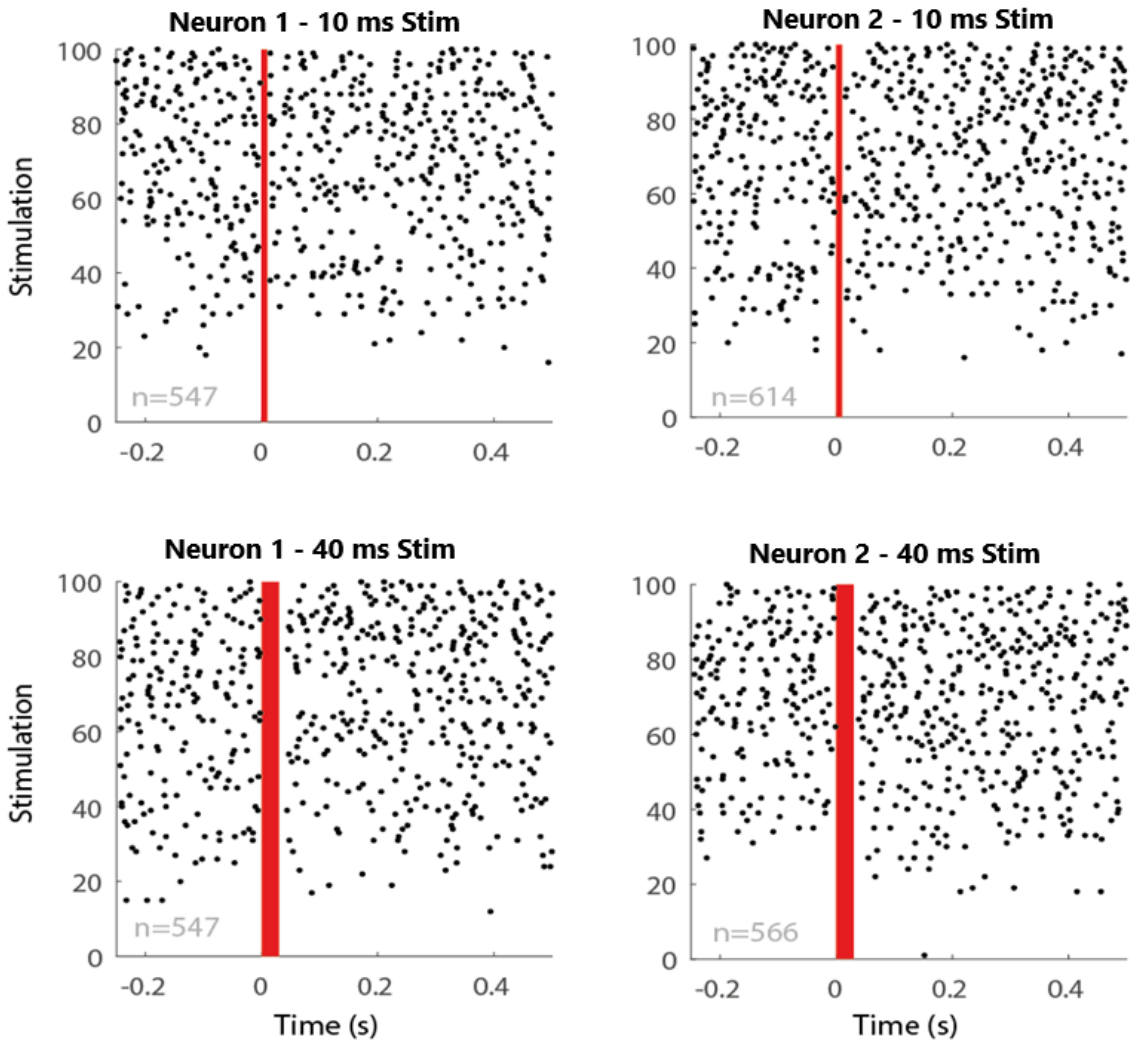

Fig. 23. *Raster plots showing the activity of two individual neurons recorded in the OFC area of GFP expressing animals in different optogenetic protocols. N = number of spikes; Red bars correspond to the stimulation period.*

Discussion

The aim of the current study was to investigate firstly how the pattern of connections from the supra- and infragranular layers of the S1 cortex project to downstream cortical areas using an adeno-associated (AAV5) viral tracing but more important how prefrontal cortex integrates and processes information from primary sensory areas in context of the sensorimotor loop. In ketamine anesthetized rats, we used viral anterograde tracing and an array of epidural micro-LEDs to excite principal neurons in S1 in distinct spatio-temporal patterns. Simultaneously, we recorded local field potentials, single and multi-unit responses in primary motor cortex, secondary motor cortex, orbitofrontal, or prelimbic cortices using high density silicon probes with up to 128 channels to describe the functional properties between circuits linking S1 (supra- and infra-granular) and downstream PFC subdivisions (M2 and OFC). Given the dual approach we employed for this experiment, the discussion will be focused on two points: first the characterization of the long range projections stemming from S1 into M2 and OFC and, secondly, the functional properties these projections have on the downstream M2 and OFC areas.

All injections sites involved superficial and deep layers of the S1, avoiding the granular layer (L IV barrels), thus this study is providing information about the efferent projection patterns of the entire supra- and infra-granular cortices of S1, but without the characterization of layer specific contributions to these downstream prefrontal areas. For anterograde tracing we used AAV5 expressing GFP to infect neurons in S1. High-resolution confocal and fluorescence microscopy was used to image fluorescent axons throughout the brain. Expression of the fluorescent proteins produced sufficient contrast to detect and image individual axons in their projection zones. We confirmed previously reported projections from the barrel cortex S1to Striatum, M1, M2 and S2), but we did not find projections to other areas such as from S1 to OFC, as described by previous studies (*Mao et al., 2011; Arronof et al., 2010)* in mice and (*Bedwell et al., 2014*) in rats. Our results, however, mimic other recent or older studies of brain wide surveys of S1 efferent connections in rat, in which a direct connection between the S1 and the OFC were not seen (*Zakiewicz et al., 2014*). Moreover, electrophysiology results from studies which investigated the propagation of evoked responses due to electrical stimulation of S1 showed orthodromic responses only related to M2 area but not to OFC subdivisions (*Golmayo et al., 2003*). Interestingly, the pattern of recorded signals seem to follow the pattern of our histological data of labeled fibers pattern in M2 area across the A-P coordinates (*fig. 24*).

The inconsistency between our data and previous results highlighting the anatomical connectivity between S1 and OFC may indeed reflect biological variability, since the bulk of previous data on S1 to OFC connectivity was obtained from mice (*Mao et al., 2011; Arronof et al., 2010*). The differences between rat studies, however, can be attributed to the variation of tracing paradigms such as tracer properties, size and the position of the tracer injection zones. The discrepancy between the results reported in this study and the results from previous mentioned data (*Bedwell at al., 2014*) could also be attributed to the fact that the latter study employed a retrograde tracing paradigm, where the injected OFC subdivisions were seen projecting to the deep layers of the S1, however the amount of labeling was sparse and may or may not involve the specific injection and stimulation areas we chose in our experiment. Another point in the discussion is that our optogenetic stimulation grid was placed over the dural surface, and it is conceivable to hypothesize that the light emitted from the LEDs did not reach the deeper layers of S1 thus never reaching the areas highlighted by the retrograde tracing study. Nevertheless, the injection and viral expression of the opsin was confined to superficial and deep layers of S1 and we expected to see the anterograde labeling of fibers from deep layers of S1 to the OFC subdivisions described by *Bedwell et al., 2014*, and a concern arises from the fact that some labeling identified by retrograde tracing may involve false positive labeling caused by contamination or uptake of tracer in passing fibers (*Zakiewicv et al., 2014*). Given this data, we can surely affirm that despite the biological variety and the variation in tracing methods employed in different studies which still leave the question open for discussion on the S1 to OFC direct connectivity, the projection of labeled fibers stemming from S1 to M2 observed in all of these studies is part of a critical cotical loop that facilitates the exchange of information between the S1 and M2 in the context of the sensory-motor loop.

Moreover, the electrophysiology results showed evoked responses in M2 area at different A-P coordinates, but not in the OFC subdivisions. This was in agreement with previous data (*Golmayo et al., 2003*) in which they showed orthodromic evoked responses across the M2 superficial and deep layers following electrical stimulation of S1, but not in OFC (*fig. 24*). Interestingly, in the same experiments, they discovered that electrical stimulation of primary visual cortex (V1) elicits evoked responses in the ventral orbital (VO) subdivision of the OFC of the rat. This area is of interest because a previous study (*Arronof et al., 2010*) showed a direct anatomical projection from mouse S1 to the VO. It is tantalizing to hypothesize that the differences we observe from our and these two studies (*Arronof et al., 2010 and Golmayo et al., 2003*) taken together highlight a distinct anatomical feature between rats and mice, however, given the low level of labeled axons present in the VO and other OFC subdivisions from S1, coupled with the fact that the two studies did not use the same methodologies it is not hard to imagine that a high order cortical area can receive direct input from both areas in both species and that the differences would be less obvious if both authors would employ the same techniques and stimulation areas.

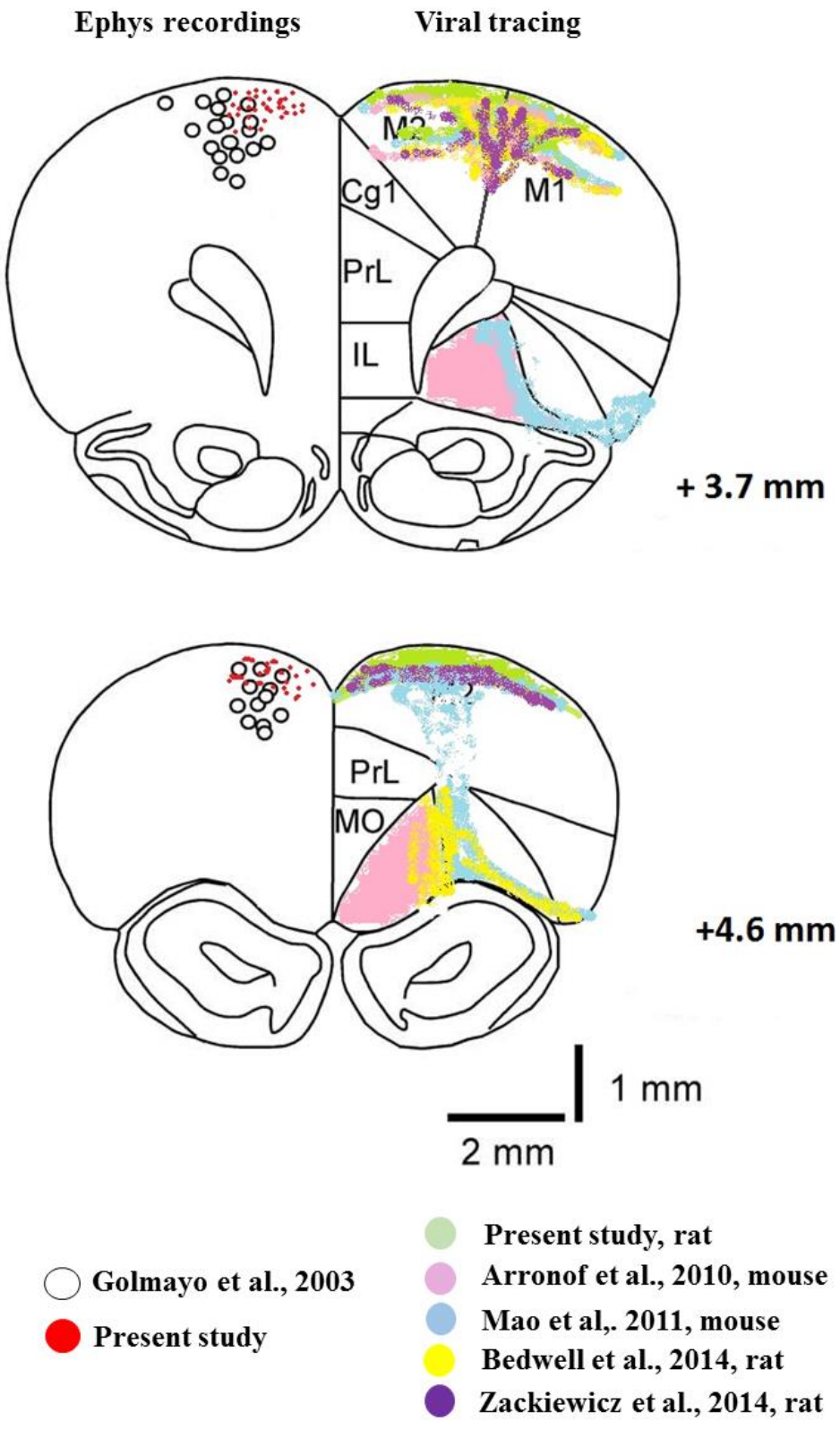

Fig. 24. *Schematic representations of recorded evoked potentials (on the left), and differences between anatomical labeling of M2 and OFC subdivisions in different studies; Paxinos and Watson, 2007.*

Our results showed evoked responses across the M2 superficial layers at different cortical depths. This was in agreement with the previous mentioned study. The amplitude of these signals varied across the length of the silicon probe which highlights a layer specificity mirrored in the histological study but also was dependent on the location probe in regards to the anatomical distribution of labeled axons in M2. The strongest evoked response we recorded were at +3.7 mm from Bregma, where subsequent histological analysis revealed an abundance of labeled fibers spread across M2 and parts of M1 (*fig. 17 A1*). However, due to the limited number of animals, we only recorded in this area only in one animal and one control, a more comprehensive study in which different recordings from different layer depths is needed for an accurate assessment of functional connectivity in these areas.

The data from *Golmayo et al., 2003* and from our study as well seems to be in agreement with the fact that the more we move in the anterior axis towards the frontal pole, the pattern of labeled fibers and evoked responses seems to follow a pattern of lateralization ending in an ordered arrangement of labeled fibers across the superficial layers of M2 all across the dorsal area (*fig. 17 A4, 24*). In more accordance with the evidence so far, the firing rate of individual neurons in OFC showed no significant difference after the optogenetic stimulation of S1. Here, two caveats deserve discussion. First, since the majority of retrograde labeled fibers from the OFC subdivisions to S1 were confined to deep layers, it is well mentioning that our stimulation grid was placed on the dural surface and light might not be able to penetrate the deep layers and influence the activity of OFC individual neurons. Thus a study which sets different optogenetic stimulations at different depths in the cortex is needed to assess the contribution of different cortical layers on the OFC subdivisions. Second, the location of the stimulation grid was chosen after the injection coordinates and it is conceivable that the grid did not cover the same areas in all animals therefore differences in LFP amplitude were due to the variability of the grid placement in the same manner we observed differences in amplitude in LFP traces due to probe placement. To overcome such predicament, intrinsic camera imaging is needed to accurately identify the BF in S1 following whisker deflection before the grid is placed on the dura.

We have performed a dual approach to our study in which we combined AAV5 directed viral tracing with optogenetic stimulation and high density silicon probe recordings in ketamine anesthetized rats expressing channelrhodopsin-2(ChR2) in primary somatosensory cortex to investigate the S1 efferent projections to high order cortical areas such as M2 and OFC and how prefrontal cortex integrates and processes information from primary sensory areas in context of the sensorimotor loop. We were able to show labeled axons arising from superficial and deep layers of S1 to M2 but not the OFC. LFP recordings were in agreement with the histological analysis and showed evoked responses all across the M2 superficial layers, but no such evoked responses were recorded in OFC. The individual firing pattern of the OFC was not influenced by the optogenetic stimulation, which is in agreement with our previous analysis.

References

Alloway, K.D. ,Olson,M.L.,and Smith,J.B.(2008).Contralateral corticothalamic projections from MI whisker cortex: potential route for modulating hemispheric interactions. J. Comp.Neurol. 510, 100–116.doi:10.1002/cne.21782;

Alloway, K.D., Zhang,M., and Chakrabarti,S.(2004).Septal columns in rodent barrel cortex: functional circuits for modulating whisking behavior. J. Comp.Neurol. 480, 299–309.doi:10.1002/cne.20339;

Brecht,M., Krauss, A.,Muhammad,S., Sinai-Esfahani,L., Bellanca,S,,and Margrie ,T.W. 2007. Organization of rat vibrissal-motor cortex and adjacent areas according to cytoarchitectonics, microstimulation, andintracellularstimulation of identified cells. J. Comp.Neurol. 479, 360–373.doi:10.1002/cne.20306;

Christian Bamann, Taryn Kirsch, Georg Nagel and Ernst Bamberg. 2008. Spectral Characteristics of the Photocycle of Channelrhodopsin-2 and Its Implication for Channel Function. J. Mol. Biol. (2008) 375, 686–694. doi:10.1016/j.jmb.2007.10.072;

Claudia Cecchetto, Mufti Mahmud, Member, EMBS & IEEE, Stefano Vassanelli. 2015. Anesthesia Effect on Single Local Field Potentials Variability in Rat Barrel Cortex: Preliminary Results. 978-1-4244-9270-1/15/$31.00 ©2015 IEEE;

Cyrille Rossant, Shabnam N Kadir, Dan F M Goodman, John Schulman, Maximilian L D Hunter, Aman B Saleem, Andres Grosmark, Mariano Belluscio, George H Denfield, Alexander S Ecker, Andreas S Tolias, Samuel Solomon, György Buzsáki, Matteo Carandini & Kenneth D Harris. 2016. Spike sorting for large, dense electrode arrays. doi:10.1038/nn.4268;

D. Öngür and J.L. Price. 2000. The Organization of Networks within the Orbital and Medial Prefrontal Cortex of Rats, Monkeys and Humans. Oxford University Press 2000. Cerebral Cortex Mar 2000;10:206–219; 1047–3211/00/$4.00.

Dirk Feldmeyer, Michael Brecht, Fritjof Helmchen , Carl C.H. Petersen , James F.A. Poulet, Jochen F. Staigeri, Heiko J. Luhmann, Cornelius Schwarz. 2013. Barrel cortex function. 0301-0082 http://dx.doi.org/10.1016/j.pneurobio.2012.11.002;

Edmund T. Rolls, Fabian Grabenhorst. 2008. The orbitofrontal cortex and beyond: From affect to decision-making. doi:10.1016/j.pneurobio.2008.09.001;

Erich Talamoni Fonoff, Jose Francisco Pereira Jr., Leonardo Valente Camargo, Camila Squarzoni Dale, Rosana Lima Pagano, Gerson Ballester, Manoel Jacobsen Teixeira. 2009. Functional mapping of the motor cortex of the rat using transdural electrical stimulation. Behavioural Brain Research 202 (2009) 138–141. doi:10.1016/j.bbr.2009.03.018;

Fabri,M., and Burton,H. 1991a. Ipsilateral cortical connections of primary somaticsensory cortex in rats. J. Comp.Neurol. 311, 405–424.doi: 10.1002/cne.903110310;

Fabri,M.,and Burton,H. 1991b. Topography of connections between primary somatosensory cortex and posterior complex in rat: a multiple fluorescent tracer study. BrainRes. 538, 351–357.doi:10.1016/0006-8993(91)90455-5;

Feldmeyer, D.,Brecht, M.,Helmchen, F.,Petersen,C.C., Poulet,J.F., Staiger,J.F.,et al..2013.Barrel cortex function. Prog.Neurobiol. 103, 3–27.doi:10.1016/j.pneurobio.2012.11.002

Frostig,R.D., Xiong,Y.,Chen-Bee, C.H.,Kasnak,E., and Stehberg,J. 2008. Large-scale organization of rat sensorimotor cortex based on a motif of large activiation spreads. J. Neurosci. 28, 13274–13284.doi:10.1523/JNEUROSCI.4074-08.2008;

Georg Nagel, Tanjef Szellas, Wolfram Huhn, Suneel Kateriya, Nona Adeishvili, Peter Berthold, Doris Ollig, Peter Hegemann, and Ernst Bamberg. 2003. Channelrhodopsin-2, a directly light-gated cation-selective membrane channel. doi10.1073pnas.1936192100;

György Buzsáki. 2004. Large-scale recording of neuronal ensembles. doi:10.1038/nn1233;

Henri J. J. M. Van De Werd Æ Harry B. M. Uylings. 2008. The rat orbital and agranular insular prefrontal cortical areas: a cytoarchitectonic and chemoarchitectonic study. Brain Struct Funct (2008) 212:387–401..doi 10.1007/s00429-007-0164-y;

Herbert P. Killackey and S. Murray Sherman. 2003. Corticothalamic Projections from the Rat Primary Somatosensory Cortex. The Journal of Neuroscience, August 13, 2003 • 23(19):7381–7384 • 7381;

Isabelle Ferezou, Florent Haiss, Luc J. Gentet, Rachel Aronoff, Bruno Weber, and Carl C.H. Petersen. 2007. Spatiotemporal Dynamics of Cortical Sensorimotor Integration in Behaving Mice. Neuron 56, 907–923, December 6. doi 10.1016/j.neuron.2007.10.007;

Izabela M. Zakiewicz , Jan G. Bjaalie and Trygve B. Leergaard. 2014. Brain-wide map of efferent projections from rat barrel cortex. doi: 10.3389/fninf.2014.00005;

James J. Jun, Nicholas A. Steinmetz, Joshua H. Siegle, Daniel J. Denman, Marius Bauza, Brian Barbarits, Albert K. Lee, Costas A. Anastassiou, Alexandru Andrei, Çağatay Aydın, Mladen Barbic, Timothy J. Blanche, Vincent Bonin, João Couto, Barundeb Dutta, Sergey L. Gratiy, Diego A. Gutniski, Michael Häusser, Bill Karsh, Peter Ledochowitsch, Carolina Mora Lopez, Catalin Mitelut, Silke Musa, Michael Okun, Marius Pachitariu, Jan Putzeys, P. Dylan Rich, Cyrille Rossant, Wei-lung Sun, Karel Svoboda, Matteo Carandini , Kenneth D. Harris, Christof Koch , John O'Keefe & Timothy D. Harris. 2017. Fully integrated silicon probes for high-density recording of neural activity. doi:10.1038/nature24636;

Jennifer M. Birrell and Verity J. Brown. 2000. Medial Frontal Cortex Mediates Perceptual Attentional Set Shifting in the Rat. The Journal of Neuroscience, June 1, 2000, 20(11):4320–4324;

Jeremy Freeman, Nikita Vladimirov, Takashi Kawashima, Yu Mu, Nicholas J Sofroniew, Davis V Bennett, Joshua Rosen, Chao-Tsung Yang, Loren L Looger & Misha B Ahrens. 2014. Mapping brain activity at scale with cluster computing. doi:10.1038/nmeth.3041;

John Y. Lin, Michael Z. Lin, Paul Steinbach, and Roger Y. Tsien. 2009. Characterization of Engineered Channelrhodopsin Variants with Improved Properties and Kinetics. Biophysical Journal Volume 96 March 2009 1803–1814;

Joseph L. Price. 2007. Definition of the Orbital Cortex in Relation to Specific Connections with Limbic and Visceral Structures and Other Cortical Regions. Ann. N.Y. Acad. Sci. 1121: 54–71 (2007). C 2007 New York Academy of Sciences. doi: 10.1196/annals.1401.008;

Jung Hoon Sul, Hoseok Kim, Namjung Huh, Daeyeol Lee, and Min Whan Jung. 2010. Distinct Roles of Rodent Orbitofrontal and Medial Prefrontal Cortex in Decision Making. Neuron 66, 449–460, May 13, 2010. doi 10.1016/j.neuron.2010.03.033;

L. Golmayo, A. Nunez and L. Zaborsky. 2003. Electrophysiological evidence for the existence of a posterior cortical-prefrontal-basal forebrain circuitry in modulating sensory responses in visual and somatosensory rat cortical areas. Neuroscience 119 (2003) 597– 609. doi:10.1016/S0306-4522(03)00031-9;

Leopoldo Petreanu, Daniel Huber, Aleksander Sobczyk & Karel Svoboda. 2007. Channelrhodopsin-2–assisted circuit mapping of long-range callosal projections.1097-6256.DOI:10.1038/nn1891;

Leopoldo Petreanu, Tianyi Mao, Scott M. Sternson1 & Karel Svoboda. 2009. The subcellular organization of neocortical excitatory connections. Vol 457 | 26 February 2009. doi:10.1038/nature07709;

Ludmilla Lokmane , Sonia Garel. 2014. Map transfer from the thalamus to the neocortex: Inputs from the barrel field. Seminars in Cell & Developmental Biology 35 (2014) 147–155. doi.org/10.1016/j.semcdb.2014.07.005;

Marius Pachitariu, Nicholas Steinmetz, Shabnam Kadir, Matteo Carandini and Kenneth D. Harris. 2016. Kilosort: realtime spike-sorting for extracellular electrophysiology with hundreds of channels. doi: http://dx.doi.org/10.1101/061481 .

Mathew E. Diamond, Ehsan Arabzadeh. 2013. Whisker sensory system – From receptor to decision. Progress in Neurobiology 103 (2013) 28–40. doi.org/10.1016/j.pneurobio.2012.05.013;

Michael A. McDannald, Michael P. Saddoris, Michela Gallagher, and Peter C. Holland. 2005. Lesions of Orbitofrontal Cortex Impair Rats' Differential Outcome Expectancy Learning But Not Conditioned Stimulus-Potentiated Feeding. The Journal of Neuroscience, May 4, 2005 • 25(18):4626 – 4632. doi:10.1523/JNEUROSCI.5301-04.2005;

Michael S Lewicki. 1998. A review of methods for spike sorting: the detection and classification of neural action potentials; Comput. Neural Syst. 9 (1998) R53–R78. PII: S0954-898X(98)84153-5;

Nicholas A Steinmetz, Christof Koch, Kenneth D Harris and Matteo Carandini. 2018. Challenges and opportunities for large-scale electrophysiology with Neuropixels probes. Current Opinion in Neurobiology 2018, 50:92–100. doi.org/10.1016/j.conb.2018.01.009;

Rachel Aronoff, Ferenc Matyas, Celine Mateo, Carine Ciron, Bernard Schneider and Carl C.H. Petersen. 2010. Long-range connectivity of mouse primary somatosensory barrel cortex. European Journal of Neuroscience, Vol. 31, pp. 2221–2233, 2010 doi:10.1111/j.1460-9568.2010.07264.x;

Sarvin Ghods-Sharifi, Desirae M. Haluk, Stan B. Floresco. 2007. Differential effects of inactivation of the orbitofrontal cortex on strategy set-shifting and reversal learning. doi:10.1016/j.nlm.2007.10.007;

Satoshi Manita, Takayuki Suzuki, Chihiro Homma, Takashi Matsumoto, Maya Odagawa, Kazuyuki Yamada, Keisuke Ota, Chie Matsubara, Ayumu Inutsuka, Masaaki Sato, Masamichi Ohkura, Akihiro Yamanaka, Yuchio Yanagawa, Junichi Nakai, Yasunori Hayashi, Matthew E. Larkum, and Masanori Murayama. 2015. A Top-Down Cortical Circuit for Accurate Sensory Perception. Neuron 86, 1304–1316 June 3, 2015 .http://dx.doi.org/10.1016/j.neuron.2015.05.006;

Sieben,K., Röder,B., and Hanganu-Opatz,I.L. 2013. Oscillatory entrainment of primary somatosensory cortex encodes visual control of tactile processing. J. Neurosci. 33, 5736–5749.doi:10.1523/JNEUROSCI.4432-12.2013;

Smith,J.B.,and Alloway, K.D. 2013. Rat whisker motor cortex is subdivided into sensory-input and motor output areas. Front.NeuralCircuits. 7:4. doi:10.3389/fncir.2013.00004;

Smith,J.B.,Radhakrishnan,H.,andAlloway,K.D. 2012. Rat claustrum coor-dinates but does not integrate somatosensory and motor cortical information. J. Neurosci. 32, 8583–8588.doi:10.1523/JNEUROSCI.1524-12.2012;

Stacey A. Bedwell , E. Ellen Billett , Jonathan J. Crofts and Chris J. Tinsley. 2014. The topology of connections between rat prefrontal, motor and sensory cortices. Frontiers in Systems Neuroscience September 2014 Volume 8 Article 177. doi: 10.3389/fnsys.2014.0017;

Takashi R. Sato and Karel Svoboda. 2010. The Functional Properties of Barrel Cortex Neurons Projecting to the Primary Motor Cortex. The Journal of Neuroscience, March 24, 2010 • 30(12):4256 – 4260. doi:10.1523/JNEUROSCI.3774-09.2010;

Tianyi Mao, Deniz Kusefoglu, Bryan M. Hooks, Daniel Huber, Leopoldo Petreanu, and Karel Svoboda. 2011. Long-Range Neuronal Circuits Underlying the Interaction between Sensory and Motor Cortex. Neuron 71, 111–123, October 6, 2011. DOI 10.1016/j.neuron.2011.07.029;

Xiao-Hua Cao, De-Heng Wang a, Jing Bai, Shao-Ci Zhou, Yong-Di Zhou. 2008. Prefrontal modulation of tactile responses in the ventrobasal thalamus of rats. Neuroscience Letters 435 (2008) 152–157. doi: 10.1016/j.neulet.2008.02.030;

Zachary F Mainen and Adam Kepecs. 2009. Neural representation of behavioral outcomes in the orbitofrontal cortex. Current Opinion in Neurobiology 2009, 19:84–91. doi 10.1016/j.conb.2009.03.010;

Zakiewicz ,I.M., vanDongen, Y.C., Leergaard,T.B.,and Bjaalie, J.G. 2011. Workflow and atlas system for brain-wide mapping of axonal connectivity in rat. PLoSONE 6:e22669. doi:10.1371/journal.pone.0022669;

Zhang,Z.W,and Deschenes,M. 1998. Projections to layer VI of the posteromedial barrel field in the rat:a reappraisal of the role of corticothalamic pathways. Cereb.Cortex 8, 428–436.doi:10.1093/cercor/8.5.428;